Department of Precision and Microsystems Engineering

Distributed vibration control for robotic cantilever beams:

Study of optimal control architectures for robotic metamaterials with relative measurements

Viktor Buskes

Report no : 2022.046
Coach : Marcin Kaczmarek
Professor : Dr Hassan HosseinNia
Specialisation : Mechatronic System Design
Type of report : MSc Thesis
Date : 17 August 2022

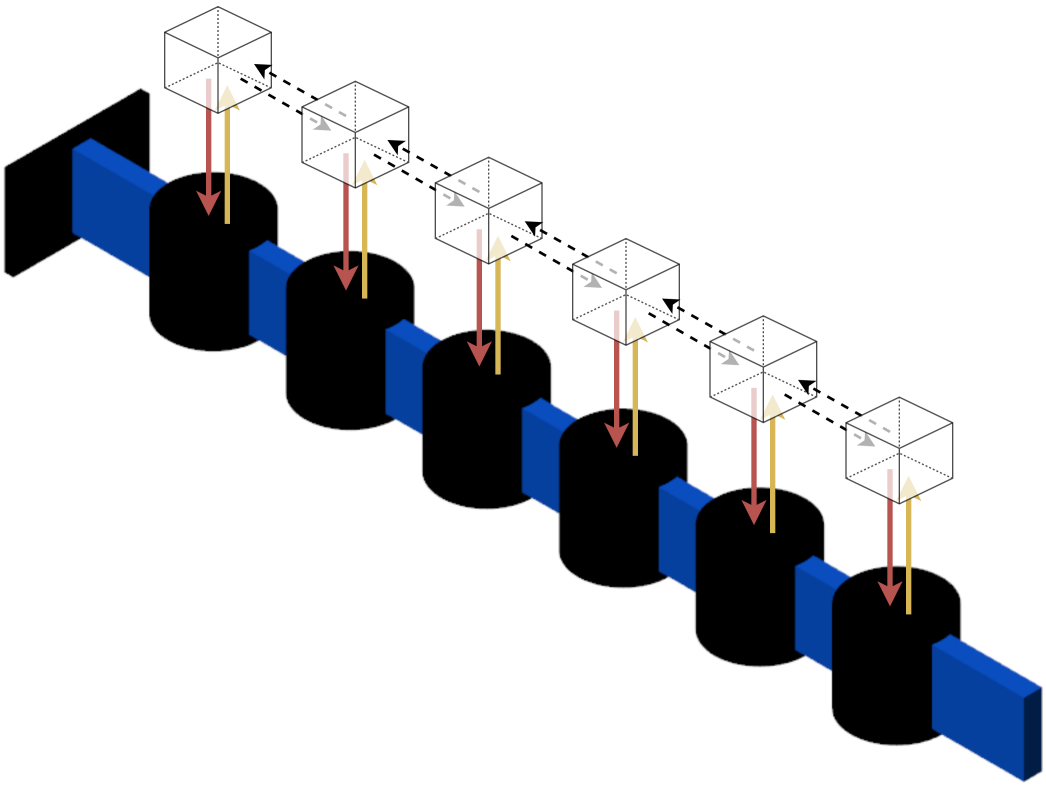

TU Delft Delft University of Technology

Challenge the future

Distributed vibration control for robotic cantilever beams:

Study of optimal control architectures for robotic metamaterials with relative measurements

Master of Science Thesis

For the Individual Double Master's Degree in Systems and Control and Mechanical Engineering at Delft University of Technology

Viktor Buskes

August 17, 2022

Faculty of Mechanical, Maritime and Materials Engineering (3mE) · Delft University of Technology

Acknowledgements

I would like to thank my daily supervisor, Marcin Kaczmarek, for his guidance and the many useful discussions we've had in our weekly meetings. Furthermore, I would like to thank Hassan HosseinNia for his kind support during the thesis project. I always felt welcome in his group to discuss various topics. Lastly, I would like to thank Sergio Grammatico for supervising the thesis from the side of DCSC and Jonas Veenstra and Corentin Coulais for welcoming me to the University of Amsterdam and allowing me to do experiments in their lab. Additional thanks to Jonas for his endless support on the experimental setup and generating useful ideas.

Delft, University of Technology
August 17, 2022

Viktor Buskes

Abstract

Vibrations and disturbances are becoming more of a concern as lightweight, flexible structures in high-tech systems are pushed towards faster speeds and higher precision. Active Vibration Control (AVC) methods have been effectively used to attenuate vibrations and increase the bandwidth of these systems. With the miniaturisation of electronics, an increasing amount of sensor and actuator pairs can be used for AVC applications. Not only does this allow for higher active damping, it also grants more flexibility in terms of control. This trend has led to the study of robotic metamaterials and meta-structures: large-scale engineered materials build out of a repeating pattern of unit cells, where each unit cell contains a sensor, actuator and sometimes even a computing unit. The optimal control architecture to use for these systems is a difficult dilemma, since decentralised and centralised control schemes both have fundamental trade-offs in terms of performance and scalability. In this paper we study distributed control, a promising middle-ground solution that is hardly used in AVC applications. We show with the use of LQR that a distributed control architecture can achieve optimal performance in the low-frequency range for robotic materials with relative measurements. Additionally, the actuators use lower maximum control forces and a distributed control architecture remains scalable for implementation in large-scale systems. In this paper the robotic cantilever beam is studied as a specific example as it represent many typical high-tech applications. Furthermore, implications on periodic robotic meta-structures are made using LQR in the Spatial Fourier Domain.

Table of Contents

Acknowledgements iii

Abstract v

1 Introduction 1

2 Background 5

2-1 Spatially invariant systems . . . 5

2-1-1 LQR in Spatial Fourier Domain . . . 6

2-1-2 LQR in Physical Domain . . . 8

2-2 LQR for robotic materials . . . 9

3 Robotic cantilever beam 11

3-1 Model . . . 11

3-2 Numerical simulations . . . 12

3-2-1 Physical domain . . . 12

3-2-2 Modal domain . . . 12

3-2-3 Truncation and stability . . . 15

3-3 Experimental validation . . . 17

3-3-1 Unit-cell structure . . . 17

3-3-2 Infrastructure . . . 17

3-3-3 Cantilever beam . . . 18

3-3-4 Results . . . 19

4 Extending the results 23

4-1 Larger pendulum systems . . . 23

4-2 Hexagonal structure . . . 26

4-3 Larger ring structures . . . 29

4-4 Matlab model . . . 31

5 Discussion & Conclusion 33

5-1 Conclusion . . . 33

5-2 Further Research . . . 34

Bibliography **37**

A System model **39**

B Additional plots **41**

C Actual gains used **45**

Chapter 1

Introduction

As lightweight systems in high-tech industry are pushed towards higher speeds and precision, their structural resonance modes start limiting the reachable bandwidth. As a result, the demand for more advanced vibration attenuation solutions is rising. Passive techniques have been used to increase damping in systems, for example, using a tuned-mass-damper [1]. However, they can add significant amount of mass to the system and only work in a narrow range of frequencies. Active Vibration Control (AVC) methods have a wider operating range and can use lightweight sensors and actuators to improve performance [2]. State-of-the-art AVC systems use piezoelectric sensors and actuators embedded onto the flexible host structure in combination with, for example, velocity feedback or positive-position feedback [3, 4]. A common testbed is the cantilever beam, which represents many typical high-tech applications like wafer grippers, leaf-springs in precision systems or flexible manipulators.

With the continuous miniaturisation and advancements of electronics, it is possible to integrate more sensors and actuators into structures and materials for vibration damping. This grants more flexibility in terms of control and can also lead to higher performance, because the observability and controllability of the vibration modes increase [5]. A further step is to also integrate computing units inside the material, creating complex engineered robotic materials [6]. In this paper we study robotic metamaterials and meta-structures as promising AVC solutions for the high-tech industry.

Metamaterials are engineered lattice structures made out of a repeated pattern of unit cells. They are often studied for their exotic properties like a negative refractive index, negative Poisson ratio and negative mass density to name a few [7]. Robotic metamaterials have a sensor, actuator and even a computing unit in each unit cell [6]. With control, these materials are versatile and exhibit interesting phenomena, like programmable bulk properties [8,9] and odd-reciprocity [10,11]. Many metamaterials are based on the assumption of an infinite lattice and therefore are impractical to implement. Meta-structures, however, are large but finite lattices where the boundary conditions also play an important role. Robotic meta-structures, like smart cantilever beams or truss structures, are promising new solutions for the vibration control industry as replacement of conventional materials.

As robotic meta-structures contain many more sensors and actuators than conventional AVC systems, a revision of the control architecture is necessary. For many meta-structures a centralised control scheme, where a single controller is connected to all the sensors and actuators (Figure 1-1a), is not an option. This would result in high computational load and extensive requirements on the communication network. A decentralised control architecture (Figure

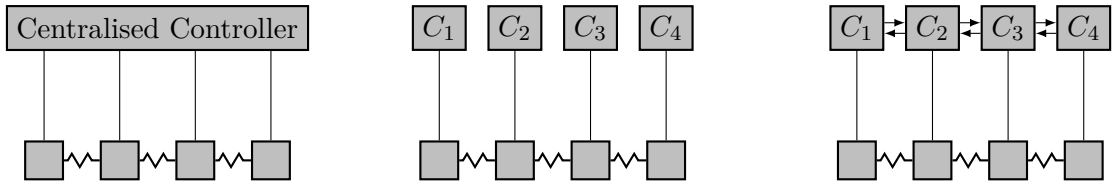

(a) Centralised controller. **(b)** Decentralised controllers. **(c)** Distributed controllers.

Figure 1-1: Three possible control architectures used on a unit cell structure.

1-1b), where each unit cell has its own independent controller, seems like the most natural option for large-scale systems. This is more easily scalable than a centralised approach, because the controllers don't require connectivity to all sensors and actuators. However, the performance and optimality are often worse as the controllers work on limited information within the system [12]. Seeking a balance between performance and scalability, it is compelling to investigate a distributed control architecture (Figure 1-1c). This scheme can improve performance by sharing information with neighbours while remaining scalable for implementation on large-scale systems. Distributed control, however, is rarely used in vibration control, let alone metamaterials.

Research in [13] and [14] provides a solid motive for the further investigation of distributed control. They prove that this scheme can reach optimal performance for systems with spatially invariant dynamics using principles of Linear-Quadratic-Regulator (LQR) and $\mathcal{H}_\infty$ control. Metamaterials are in essence spatially invariant systems and it is reasonable to assume that many meta-structures also exhibit spatially invariant dynamics, although in a weaker form due to the boundary conditions. Therefore, studying the potential of a distributed control architecture for these cases is convincing.

However, for vibration control, the theory is not applicable yet as the distributed controllers in [13] are obtained with absolute measurements in mind. This is relevant for, for example, large vehicle platoons. For vibration control systems this is more difficult to implement as they usually have to operate with relative measurements from strain gauges or piezoelectric sensors. Furthermore, the distributed controllers are obtained by penalising the entire frequency range. In AVC applications this is not always wanted as damping of lower order modes is more significant. It is unknown whether the strengths of distributed control will still hold in these different circumstances.

In this paper we study the feasibility of distributed control for robotic materials with relative measurements. More specifically, using LQR it is examined whether the optimal control architecture remains distributed with relative measurements and if it results in better damping performance compared to decentralized control. In this paper we apply this theory first and foremost on a robotic cantilever beam. This is not only a practical configuration for the high-tech industry, but also provides a balanced mix between theory on meta-structures and conventional cantilever beams with AVC. Additionally, we apply the theory on periodic structures using the Spatial Fourier Domain, which gives new insights into the controller design of larger structures and metamaterials.

The paper is structured as follows: background information on spatially invariant systems, LQR and control architectures will be given in Section 2. The model of the robotic cantilever beam is given in Section 3, along with the numerical simulation and experimental validation. In Section 4, the work is extended to larger systems and circular systems. The paper ends with a discussion and conclusion in Section 5.

Chapter 2

Background

In this section, background information is given on spatially invariant systems and their optimal control using LQR. The implications of this theory for robotic metamaterials and meta-structures will be given. Lastly, small changes are given that make the theory applicable for AVC applications.

2-1 Spatially invariant systems

Many large-scale systems can be described as similar units interacting mostly with nearest neighbours only. Examples of discrete systems are vehicle platoons, formation flights or series of mass-spring systems. Also lumped approximations of partial differential equations fit this description. For example, slender beams with equally spaced collocated sensors and actuators or thermodynamic problems. When such systems have an infinite amount of units or the units interact in a circular manner, they can be regarded as spatially invariant as the dynamics is independent of spatial location. The control architecture to control such systems has been a thoroughly studied field of research [12–21]. Because spatially invariant systems have large dimensions, optimal centralised control techniques like LQR and Model-Predictive-Control are often not feasible. This is because the optimal solution cannot be computed and the implementation is difficult. Decentralised controllers, on the other hand, are a more intuitive solution as they are only dependent on a local sensor in the system. Therefore optimisation and implementation are much more practical. However, performance is often worse, because the optimisation is only based on limited information within the system.

Research done on spatially invariant systems in the Spatial Fourier Domain, where the analysis is reduced to a single unit, sparked the interest in distributed controllers [13]. Namely, by computing an optimal LQR feedback matrix in Spatial Fourier Domain and then converting it back to physical domain, it was proven that the optimal control structure of spatially invariant systems is distributed. Not only can optimal performance be reached with this architecture, the controllers remain scalable for implementation on large-scale systems as they are only dependent on a small group of sensors.

2-1-1 LQR in Spatial Fourier Domain

The proof makes use of LQR, which is an optimal control method that minimises the quadratic objective function in Equation 2-1 for a linear system. The Q and R matrices are used to tune the response of the closed-loop system. Usually they are chosen as diagonal matrices $Q = q\mathbf{I}$ and $R = r\mathbf{I}$. High values for q penalise high state deviations, whereas a high r penalises high control inputs.

$$\begin{aligned} J &= \int_0^\infty (x^T Q x + u^T R u)\mathrm{dt} \\ \text{s.t.} \quad & \dot{x} = Ax + Bu \end{aligned} \tag{2-1}$$

The objective function is minimised by solving the Algebraic-Riccati-Equation (ARE) in Equation 2-2.

$$A^T P - PA - PBR^{-1}B^T P + Q = 0 \tag{2-2}$$

If the system is controllable it is possible to find a positive definite solution P with stabilizing feedback control $u = -Kx = -R^{-1}B^T Px$. The feedback matrix K, which is a centralised controller, provides the optimal gains for all sensors and actuators in the system. The structure of this matrix can be visualised by plotting the magnitude of the gains from a top-down view with a colour gradient. Notably, if all or most non-diagonal entries are zero, the optimal centralised feedback matrix can instead be implemented by multiple decentralised or distributed controllers, see Figure 2-1

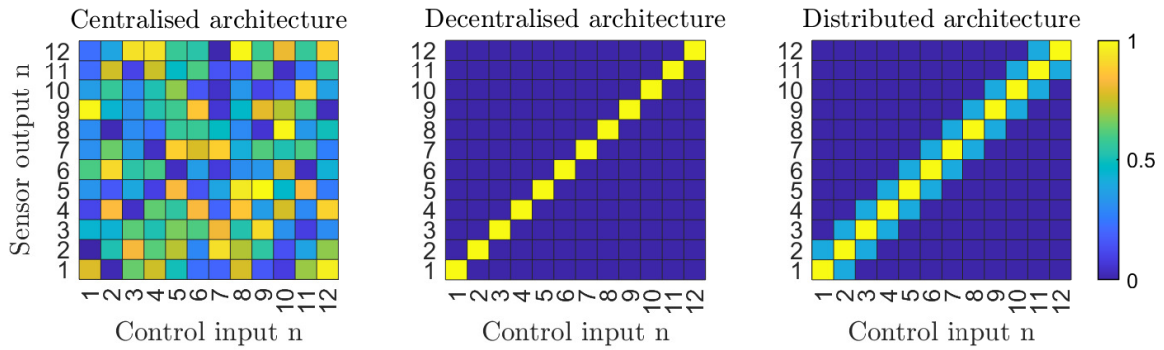

Figure 2-1: Different types of control architectures in the optimal gain matrix K.

However, since spatially invariant systems have infinite dimensions, it is impossible to compute the stabilising solution P. Therefore the proof continues in the Spatial Fourier Domain, which transforms the system to finite dimensions. Consider for example an infinite chain of mass-spring systems as shown in Figure 2-2. Here each unit cell can measure its absolute displacement x_n and velocity $\dot{x}_n$ and apply an actuator force u_n.

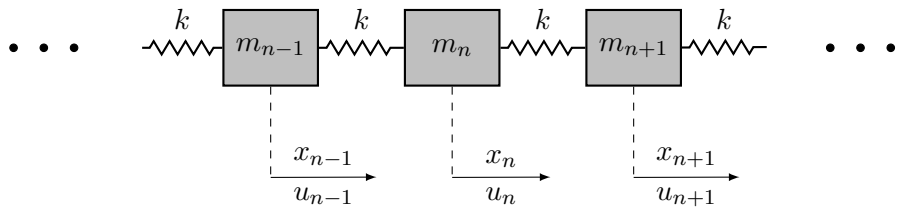

Figure 2-2: Infinite chain of mass-spring systems considered as spatially invariant system.

This system can be described by a 2x2 state space by using the shift operator T, where $T_1 x_n = x_{n+1}$ denotes the spatial index operation to the right [17], see Equation 2-3.

$$\begin{bmatrix} \dot{x}_n \\ \ddot{x}_n \end{bmatrix} = \begin{bmatrix} 0 & 1 \\ (T_1 + T_{-1} - 2)k/m & 0 \end{bmatrix} \begin{bmatrix} x_n \\ \dot{x}_n \end{bmatrix} + \begin{bmatrix} 0 \\ 1/m \end{bmatrix} u_n \tag{2-3}$$

By using the discrete Spatial Fourier transform over the unit circle $\hat{x}(t,\theta) = \sum_{-1}^{1} x(t,n)e^{-j\theta n}$ the system in Equation 2-4 can be obtained, where θ is the spatial frequency [17].

$$\begin{bmatrix} \dot{\hat{x}}_\theta \\ \ddot{\hat{x}}_\theta \end{bmatrix} = \begin{bmatrix} 0 & 1 \\ (2\cos(\theta) - 2)k/m & 0 \end{bmatrix} \begin{bmatrix} \hat{x}_\theta \\ \dot{\hat{x}}_\theta \end{bmatrix} + \begin{bmatrix} 0 \\ 1/m \end{bmatrix} \hat{u}_\theta \qquad \text{for} \quad \theta \in [0, 2\pi) \tag{2-4}$$

The system dynamics is reduced to only 2 states in Spatial Fourier Domain, which means that the ARE is solvable again. An optimal LQR controller can be computed, which stabilizes the system for all $\theta \in [0, 2\pi)$ [17]. It needs to be converted back to physical domain using the inverse Fourier transform $K = \int_0^{2\pi} \hat{K} e^{j\theta n} \mathrm{d}\theta$. The optimal centralised matrix is then a convolution of all the spatial locations $u = \sum_\zeta K(n-\zeta)x(t,\zeta)$ [21]. By plotting the values of the feedback matrix in 3D space, the final step of the proof is completed. This has been done in Figure 2-3 for 100 masses. The tuning matrix Q is chosen as $\begin{pmatrix} 0 & 0 \\ 0 & 1 \end{pmatrix}$ resulting in direct velocity feedback only. Two different values for r are compared: $r = 10^1$ and $r = 10^5$. Note that this result will be slightly sub-optimal as the result for an infinite system is used on a system of 100 masses.

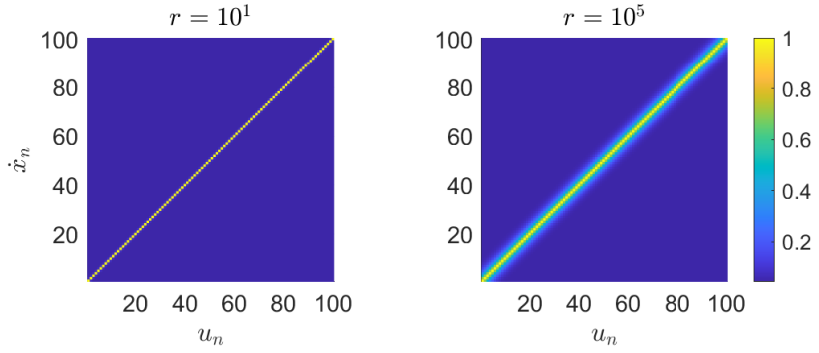

Figure 2-3: The optimal feedback matrices for a large-scale system using the Spatial Fourier Domain show decentralised/distributed architectures.

Even though there are 10,000 entries in the feedback matrix, it is evident that only the diagonals are of interest. For high control forces, i.e. low r, the optimal architecture to damp a series of mass-spring systems is to use decentralised velocity feedback controllers. This means that optimal performance can be obtained without requiring connectivity to all sensors and actuators. This will save cost, reduce implementation time and make the system more modular and scalable [22]. Many actuators, however, have limited actuator force and saturation limits need to be taken into account. When r is increased for this reason, it is beneficial to include neighbour information in the control inputs as can be seen from the upper and lower diagonal entries. This means that the optimal control architecture is distributed for systems with limited control force.

2-1-2 LQR in Physical Domain

The proof of [13] uses LQR in the Spatial Fourier Domain to control systems of infinite size. However, distributed control is still viable and effective for smaller systems with boundary conditions, as long as they contain similar units interacting mostly with nearest neighbours only. This is shown in [12], where a LQR controller is computed in the physical domain for a series of mass-spring systems clamped on both sides. For example, consider a system of 12 masses, which means that 24 states are present. In Figure 2-4 LQR is optimized to penalise all velocity states with $Q = \begin{pmatrix} \mathbf{0} & \mathbf{0} \\ \mathbf{0} & \mathbf{I} \end{pmatrix}$ to obtain only velocity feedback. In the left figure, r is chosen as $R = 10^1\mathbf{I}$, while in the right figure r is chosen as $R = 10^4\mathbf{I}$. Evident from Figure 2-4 is that for even relatively small-scale systems with boundary conditions, similar conclusions can be drawn. Namely that for actuators with limited force, it is beneficial to include neighbour information in the control inputs.

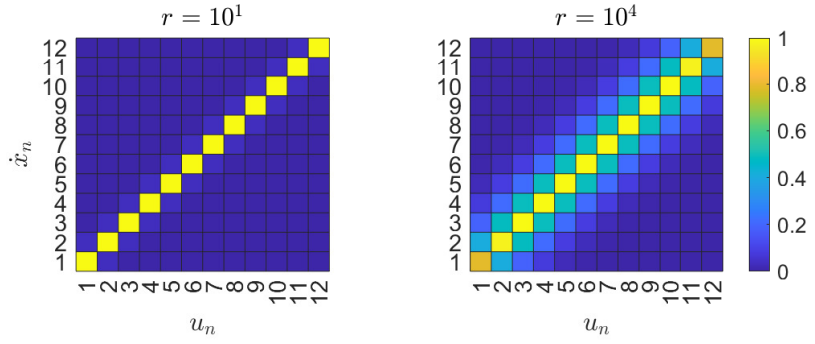

Figure 2-4: Optimal LQR matrices for finite mass-spring systems also have a decentralised/distributed control architecture.

2-2 LQR for robotic materials

Many metamaterials are modelled as infinite series of mass-spring systems. Therefore they are in essence also spatially invariant. In fact, many similar concepts like the Spatial Fourier Domain have been used to describe the behaviour of metamaterials as a continuum, like the Bloch-Floquet theorem [23]. The strength of the given background theory is the use of LQR in the Spatial Fourier Domain, which can be used on large metamaterial structures or periodic systems to simplify the control design. Furthermore, the background theory gives solid reasons for using distributed control for both metamaterials and meta-structures, which is not common in state-of-the-art literature on AVC.

However, a major difference between the given examples and vibration control applications is that absolute measurements are usually not available. For vibration control, often only relative measurements are available as embedded sensors and actuators are used, like strain gauges and piezoelectric sensors. Whether distributed control is still the optimal control strategy for spatially invariant systems with relative measurements is unknown. Furthermore, by penalising all the velocity states in physical domain the whole frequency range is minimised. This is also the case in the Spatial Fourier Domain by considering θ from 0 to 2π. Especially for AVC applications, the theory needs modifications to see if distributed control is also beneficial for more specific frequency ranges.

Chapter 3

Robotic cantilever beam

In this section, the feasibility of a distributed control architecture will be validated with relative measurements. The vibration control system of concern is a cantilever beam build out of unit cells with torque-actuated joints. This is a relevant configuration, since it is a mix between state-of-the-art meta-structures and cantilever beams. A model will be derived and numerical simulations using LQR will be performed in both physical and modal domain. At the end, the numerical simulations will be verified with an experimental setup.

3-1 Model

To validate the effect of a distributed control architecture with relative measurements the robotic cantilever beam is studied. The model is based on the schematic in Figure 3-1. The blue beams have length l and are assumed rigid. The joints can measure the relative angular displacement θ_n and apply a control torque τ_n. They have a mass m_n and rotational stiffness k.

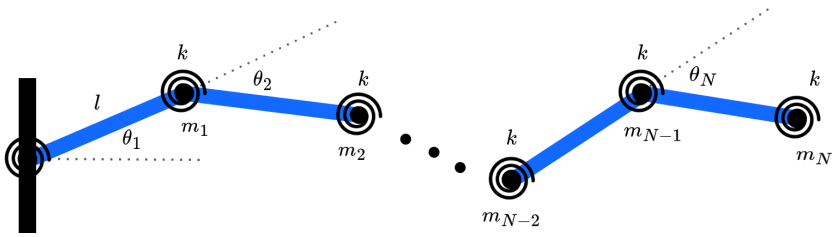

Figure 3-1: Robotic cantilever beam with relative coordinates and torque-actuated joints.

A linear, algebraic model is constructed according to a n-pendulum model where gravity is neglected. This is done by defining the displacements of each unit cell in terms of relative angular displacements θ_n, see Equation A-1 in the Appendix. The velocities can be obtained by taking the Jacobian and multiplying with the derivatives of the rotations $\dot{\boldsymbol{u}} = \nabla \boldsymbol{u} \cdot \dot{\boldsymbol{\theta}}$. The Lagrangian is defined using the kinetic and potential energy in the system $L = T - V$ where $T = \frac{1}{2} m \dot{\boldsymbol{u}}^T \dot{\boldsymbol{u}}$ and $V = \frac{1}{2} k \sum_1^N \theta_n^2$. The mass and stiffness matrices are derived with Equation 3-1.

$$\mathbf{M} = \frac{\partial T}{\partial \dot{\boldsymbol{\theta}} \partial \dot{\boldsymbol{\theta}}} \qquad \mathbf{K} = \frac{\partial V}{\partial \boldsymbol{\theta} \partial \boldsymbol{\theta}} \tag{3-1}$$

The system will be linearized around the zero equilibrium and the following values will be used: $l = 0.075$ m, $m = 0.2$ kg and $k = 0.048$ Nm/rad. For this report, N is taken as 6, which is relatively small but allows for intuitive analysis of the results. For the derived mass, stiffness and damping matrices, see Equations A-2 and A-3 in the Appendix.

3-2 Numerical simulations

3-2-1 Physical domain

It is straightforward to compute the optimal LQR matrix in physical domain by solving the ARE and using the solution as part of the optimal feedback matrix. The solution for penalising all velocities with $Q = \begin{pmatrix} \mathbf{0} & \mathbf{0} \\ \mathbf{0} & \mathbf{I} \end{pmatrix}$ and two different $R = r\mathbf{I}$ can be seen in Figure 3-2. From both figures it can be concluded that the architecture is fully decentralised, independent of the value of R. This result is contrary to earlier simulations with absolute measurements.

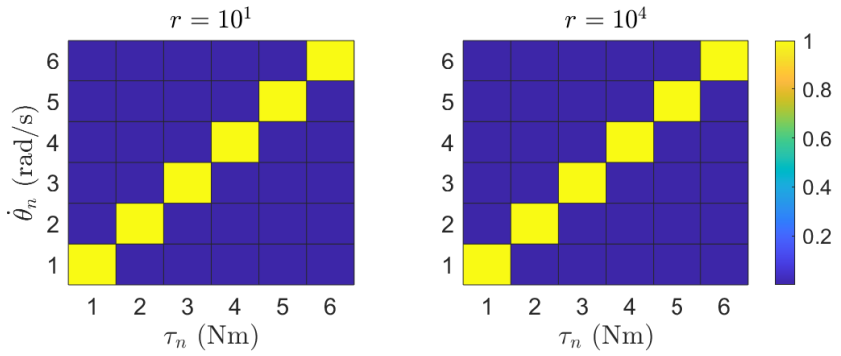

Figure 3-2: Tuning a system with relative measurements in physical domain results in a decentralised architecture, regardless of r.

An initial explanation for this could be that the relative measurements already include a form of neighbour information as opposed to absolute measurements. The physical domain, however, doesn't give great insights into why this structure really is decentralised. Furthermore, it can be troublesome to get the desired behaviour from the closed-loop system as tuning in physical domain targets the whole frequency range and gives no insights into the modes and frequency characteristics of the system. For some AVC applications, an "optimal" solution is one that mainly tackles low-order resonance modes while the higher order modes can be neglected.

3-2-2 Modal domain

The conversion to modal coordinates is done by multiplying the mass and stiffness matrices with the eigenmodes ϕ of the system, which are obtained through the eigenvalue problem $\det(K - \omega^2 M) = 0$.

$$\tilde{M} = \phi^T M \phi \qquad \tilde{K} = \phi^T K \phi \tag{3-2}$$

In modal domain, the tuning of the closed-loop system should be more intuitive, because specific modes can be penalised with the Q matrix. Furthermore, in modal domain it is possible to visualise the mode shapes and compute the LQR feedback matrix to damp each mode. However, before any physical meaning can be extracted from the LQR matrices, they need to be converted back to the physical domain by multiplying with the inverse of the mode shapes.

$$K_{\text{physical}} = K_{\text{modal}}\phi^{-1}. \tag{3-3}$$

The result for all six modes is shown in Figure 3-3. The mode shapes and the rotational direction of each unit cell give well-founded reasons for why the optimal architecture in physical domain is decentralised. Namely, by penalising all the velocities in physical domain the whole frequency range is targeted, which means that all modes tend to be minimised. However, various modes have contradictory optimal control strategies. For example, for the first mode all angular rotations are counterclockwise. As a consequence, the feedback gains are all positive as indicated in the corresponding 1st mode LQR matrix. However, higher order modes have alternating counterclockwise and clockwise rotations. This also means that the gain matrices have both positive and negative gains on the non-diagonal entries. When all modes are penalised, the summation of these feedback matrices quickly leads to the non-diagonal terms adding up to zero. The only entries in each mode that are not contradictory are the positive diagonal entries. In other words, to satisfy both the lower and higher order modes, decentralised control is the only feasible control strategy.

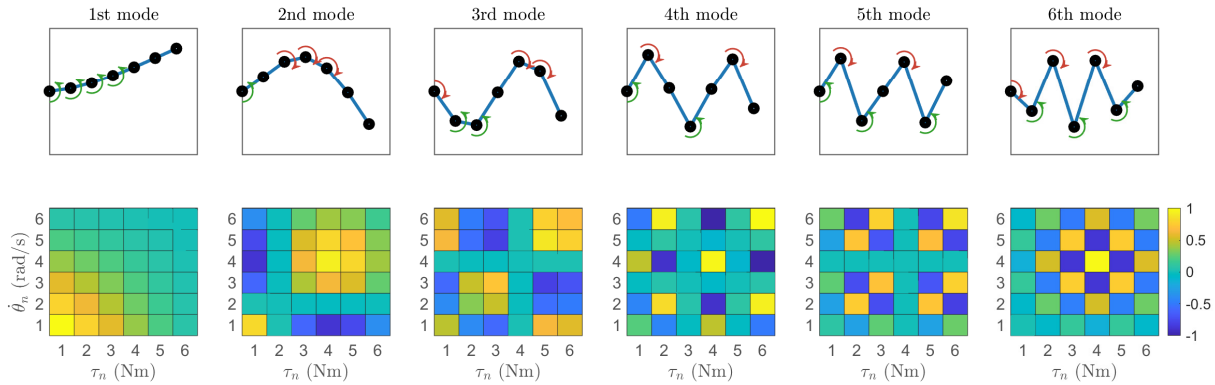

Figure 3-3: The six different modes of the system visualised, along with the optimal feedback matrix to damp each mode.

However, if not all modes are penalised using the Q matrix, non-diagonal terms will appear. For a distributed controller to be optimal, the first upper and lower diagonals need non-zero entries. When all penalised modes have positive upper and lower diagonals, the summation of these entries doesn't lead to zeros. This is equivalent to all groups of three unit cells having the same rotational direction. The first four modes have many groups of three with all rotations in the same direction, except for unit cell 1 and 2 in the third and fourth mode. It is likely that penalising the first four modes works well with a distributed controller with positive neighbour gains. But penalising higher order modes with this controller, like the fifth and sixth mode, won't be beneficial, because it would require negative neighbour gains instead.

Above assumptions can be verified by computing two LQR matrices. The first penalises all modes with $Q = \mathbf{I}$ and $R = 3.5e5\mathbf{I}$ in Figure 3-4a. The second example penalises the first four modes more heavily with $Q = \text{diag}(5, 5, 5, 3, 1, 1)$ and $R = 9e5\mathbf{I}$ in Figure 3-4b. It can be seen that the matrix is indeed fully decentralised when all modes have to be minimised. However, LQR suggests a mostly distributed control architecture as optimal structure when the first four modes are mainly penalised. This seems to verify the claims made earlier.

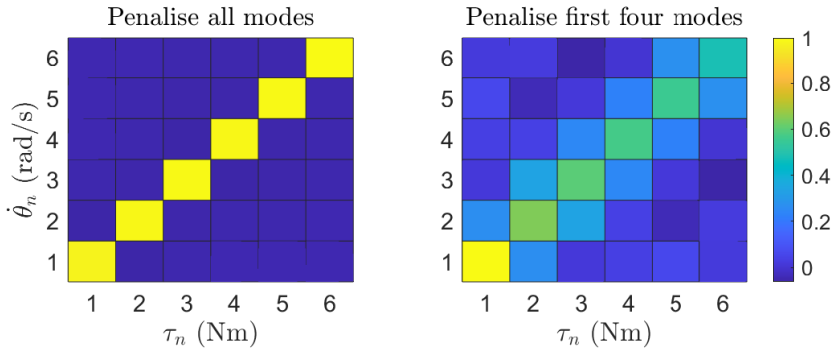

Figure 3-4: Depending on which modes are penalised, the structure of the feedback matrix is significantly different.

Both feedback matrices are simulated by means of a torque-impulse response on the first unit cell. The control input in both cases is scaled to be roughly equal such that the comparison is fair. This is done according to three energy metrics:

1. Maximum control torque in the system
2. Summation of the absolute control inputs
3. Summation of the control inputs squared

The first and last metrics give an insight into the efficiency of the algorithm. The second metric mainly determines the absolute energy put into the system. As can be seen from Figure 3-5, penalising all modes isn't necessarily the most optimal choice as the closed-loop system experiences longer settling times and higher magnitude oscillations. In the Bode plot the frequency responses of the closed-loop systems show that the distributed controller performs very well for the first four lower order modes. The fifth and sixth mode are better damped with a decentralised controller. This is in agreement with the mode shapes and optimal LQR matrices presented in Figure 3-3. The control metrics are given in Table 3-1. It can be seen that although more energy is put into the system, the distributed controllers are much more efficient. The maximum control torque in the system is reduced by almost 27%.

	All modes	First four modes
Max τ_n	6.3 mNm	4.6 mNm
$\sum \lvert u_n \rvert$	0.33 J	0.38 J
$\sum u_n^2$	1.67e-4	1.59e-4

Table 3-1: Input energies for the impulse response show that distributed controllers are more efficient than decentralised controllers.

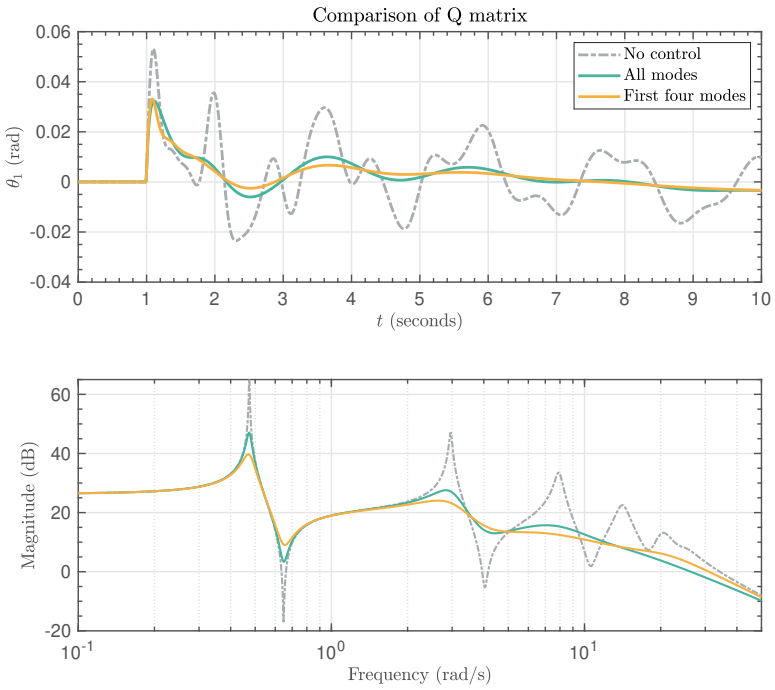

Figure 3-5: Time response (top) and frequency response (bottom) of the two closed-loop systems compared to the uncontrolled system.

There are multiple conclusions to draw from this strong result. First of all, distributed controllers have better damping capabilities than decentralised controller for the low-order modes. This makes them favourable for many active vibration control applications where damping of the first few modes is required. Because each controller is only dependent on three sensors in the system, it also remains practical for implementation in large-scale systems. Furthermore, the controllers are much more efficient, which makes them suitable for smaller and more lightweight actuators with lower actuator forces. And since the optimality is proven in modal domain, the stiffness and mass values of the system will not influence the results as the mode shapes are independent of both.

3-2-3 Truncation and stability

Before the result can be implemented on an experimental setup, the optimal feedback matrix in Figure 3-4 needs to be truncated. This must be done as it still contains off-diagonal entries with small gains. In Figure 3-6b all entries are removed except the self-gains. In Figure 3-6c also the first neighbour gains are included. However, since the off-diagonal entries are so small the performance of the truncated feedback matrix is nearly identical to the full LQR matrix, see Figure B-1 in the Appendix.

Truncation should generally be done with care, because removing off-diagonal entries can lead to unstable closed-loops. With a stability analysis it can be shown that distributed controllers with first neighbour couplings are not unconditionally stable as opposed to decentralised controllers [2]. Consider, for example, the ratio of the self-gain g_s and the neighbour gain g_n. In the truncated matrix the ratio $g_s : g_n$ is between 2 and 3 depending on which unit cell you

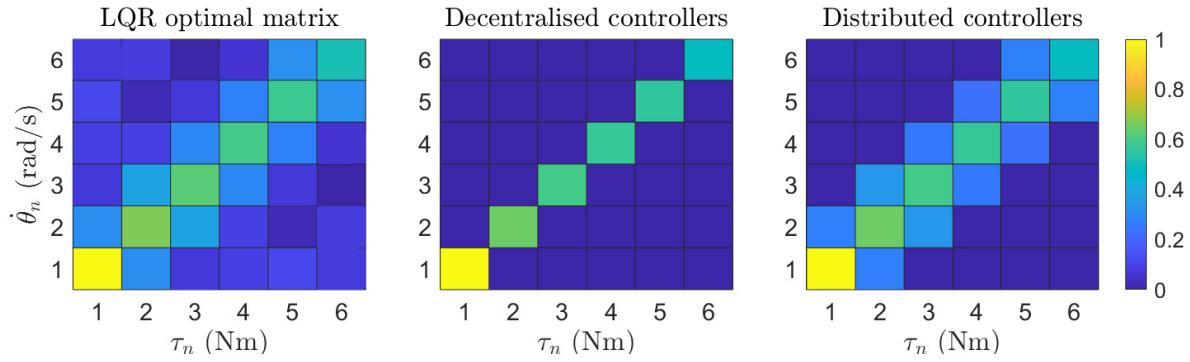

(a) The full LQR matrix. **(b)** Decentralised controllers. **(c)** Distributed controllers.

Figure 3-6: Through truncation of the optimal centralised LQR matrix, a decentralised and distributed architecture are obtained.

consider, which still results in a stable closed-loop. By manually varying this ratio, it can be determined when distributed controllers lead to an unstable system. For this analysis all six controllers have equal gains so that the stability problem reduces to only two variables: g_s and g_n. The stability region is shown in Figure 3-7 for 10,000 different gain ratios. If the real part of the closed-loop poles is negative, the system is stable and the area of the graph is marked dark grey. If not, then the area is marked light grey. It turns out that for a ratio of gains $-1.25 < g_s : g_n < 1.45$ the system will become unstable. Without any passive damping in the simulation this ratio changes to $-1.6 < g_s : g_n < 1.8$. Any centralised LQR matrix might have an unstable ratio of $g_s : g_n$, but the off-diagonal terms would then compensate for this. By removing these entries the high neighbour gains are too aggressive and destabilise the system. This happens specifically for the fifth and sixth mode, which require negative neighbour gains to be damped efficiently. On the other hand, too high negative neighbour couplings, will destabilise the lower order modes.

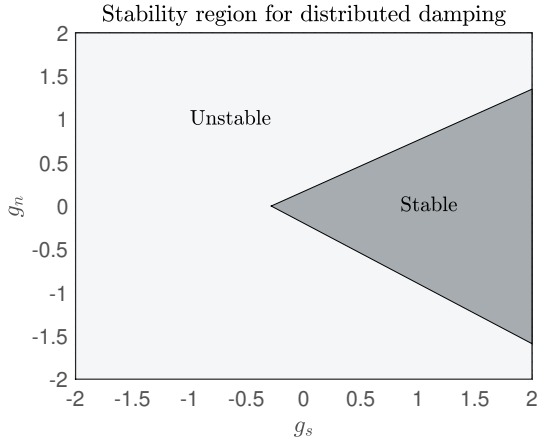

Figure 3-7: Stability region for distributed controllers with varying self-gain and neighbour-gain. The neighbour gain can't be taken too high as it leads to an unstable system.

3-3 Experimental validation

Based on the numerical simulations the potential of distributed controllers is high. They show better performance for a lower maximum control force. Furthermore, they remain scalable like decentralised controllers. To verify the numerical simulations, distributed controllers are also experimentally validated for the robotic cantilever beam of six unit cells.

3-3-1 Unit-cell structure

To construct the robotic cantilever beam with torque-actuated joints, the unit cell structure shown in Figure 3-8 is used. Each unit cell has a DC motor (black) that can measure the relative angular displacement of the rotor θ_n and apply a torque τ_n. The unit cells can be rigidly connected to each other with blue 3D-printed beams. This ensures that the distance between unit cells remains constant and the torque of the motor is transferred to neighbouring unit cells. A torsional spring can be attached on top of each rotor in the form of a rubber band, see Figure 3-9 for reference. For small angles, the spring force is only dependent on the relative angular displacement, i.e. $\tau_{\text{spring},n} = k\theta_n$. Each unit cell has a microcontroller installed under the DC motor. This can control the unit cell and is also able to send information to its first left and right neighbours through a wired connection. The maximum torque $\tau_{\max}$ of the motor is 12 mNm, the mass m of each unit cell is 0.2 kg and the torsional spring stiffness k is around 48 mNm/rad. The distance l between unit cells from rotor to rotor is 75 mm. The communication speed and sampling rate of the system is set to 100 Hz. This is around 20 times higher than the expected maximum frequency content of the system.

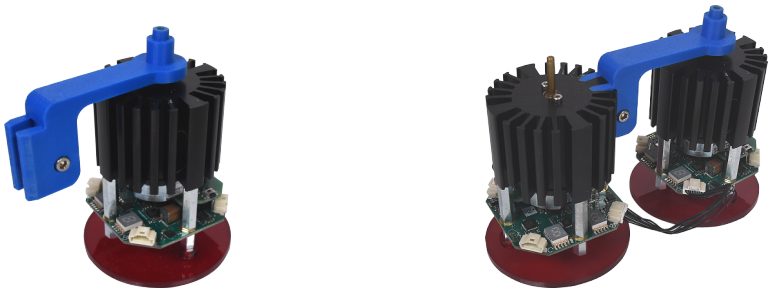

Figure 3-8: Unit cell structure with DC motors and rigid link (torsion spring left out).

3-3-2 Infrastructure

The DC motors measure the angular displacement at a rate of 100 Hz using the built-in encoder, which is sent through a digital low-pass filter with cut-off frequency at 5 Hz. The velocity is obtained on the microcontroller by storing the old sensor output and calculating the difference with the new sensor output. Simultaneously, the angular displacement is received from left and right neighbours, which is used to calculate the neighbour velocities. There is no guarantee that the angular displacements sent from the neighbours is from the exact same time frame as the local output, because of communication delays. This delay effect is mitigated as much as possible by having the sampling rate as high as possible. However, sampling rates higher than 100 Hz resulted in communication failures between unit cells.

3-3-3 Cantilever beam

By clamping six unit cells in the correct configuration, the robotic cantilever beam is obtained as shown in Figure 3-9. Note that the seventh motor is not controlled and purely adds mass at the end of the system. The robotic structure lies on a horizontal air-table to ensure high vertical stiffness and low friction in traverse directions. Note the added torsional spring for each unit cell in the form of a rubber band.

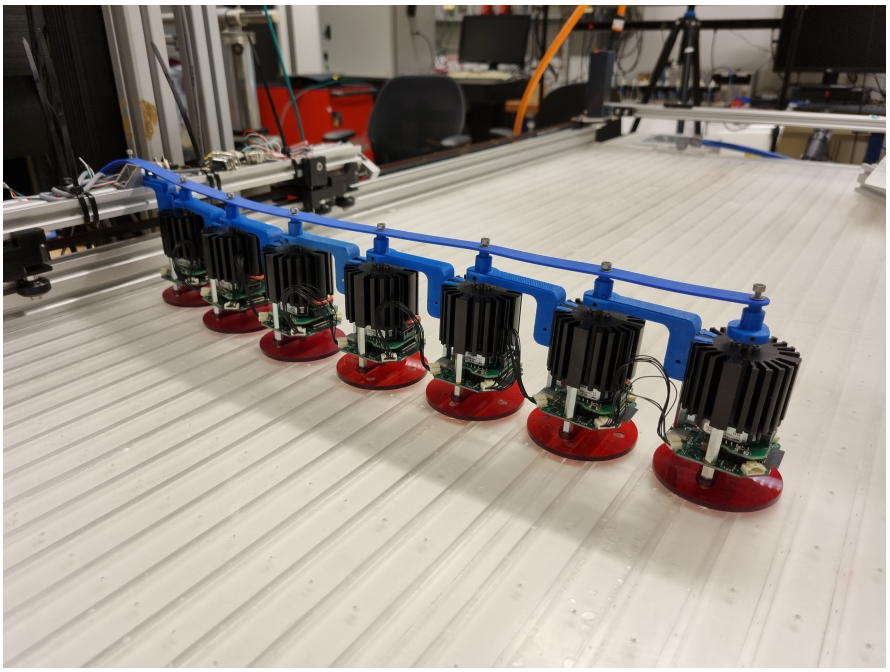

Figure 3-9: Experimental setup of the cantilever beam on the air-table. Clamped on one side to a motion stage.

The beam is clamped on one side to a motion stage. This can be moved to the left and right and is used to disturb the system. It is possible to program the motion stage with a desired amount of displacement, speed, acceleration and deceleration. However, only 10 commands can be given to the motion stage at a time, which means that frequency sweeps are not possible. Constant frequencies are possible by setting a forward and backward command and allowing the system to endlessly cycle between these two commands.

Two different perturbations are tested to validate the numerical simulations: a step input and an oscillating perturbation that excites the second mode of the system. For both scenarios the truncated decentralised controller of Figure 3-6b and truncated distributed controller of Figure 3-6c will be used and compared to each other. The maximum gains are chosen such that the forces are below saturation and the three control metrics are roughly equal.

3-3-4 Results

Step response

A step response is carried out by moving the motion stage 100 mm with a speed of 500 mm/s and an acceleration and deceleration of 5000 mm/s^2, see Figure 3-10. The aim of this perturbation is to excite as many modes and frequencies as possible. The angular deviation of the last unit cell and additionally the summation of all angular displacements can be seen in Figure 3-11. The control inputs of the experiment are shown in Table 3-2.

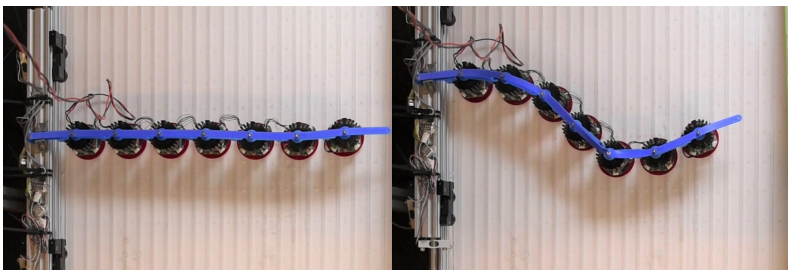

Figure 3-10: Visualisation of the beam in rest and after being perturbed.

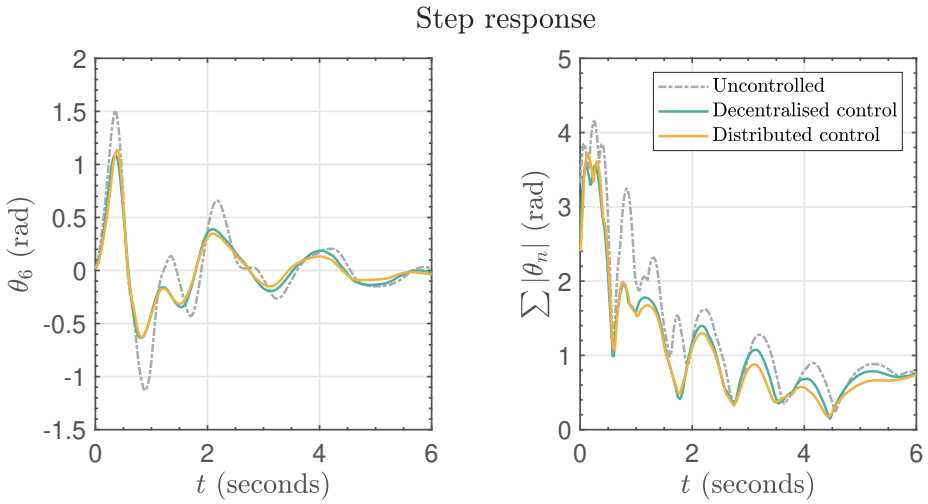

Figure 3-11: Step response of the last unit cell and summation of all unit cells. Distributed controllers have slightly lower magnitudes.

	Decentralised control	Distributed control
Max τ_n	8.9 mNm	6.8 mNm
$\sum \lvert u_n \rvert$	100 J	106 J
$\sum u_n^2$	17.7	18.7

Table 3-2: Control metrics for the step response experiment.

The same strong conclusions as for the numerical simulations can be drawn. For roughly similar control inputs the distributed controllers are able to get smaller peaks in the response and a faster settling time. The biggest difference is the maximum control torque in the system, which is 24% lower for the distributed control architecture. The major differences in the simulation and experimental setup are the irregularities in the air-table and the higher friction and damping due to this. Furthermore, larger angles are used, which might induce non-linear dynamics and damping. The experiment was repeated three times to ensure that the variance between different experiments was low, see Figures B-4 and B-5 in the Appendix.

Oscillating perturbation

Secondly, the system is perturbed at a constant frequency at which only the second mode was present. The motion stage is programmed to move at a speed of 50 mm/s, acceleration and deceleration of 1200 mm/s^2 and a back-and-forth displacement of 50 mm, see Figure 3-12. The summation of all angular rotations is recorded and given in Figure 3-13. The control inputs are given in Table 3-3.

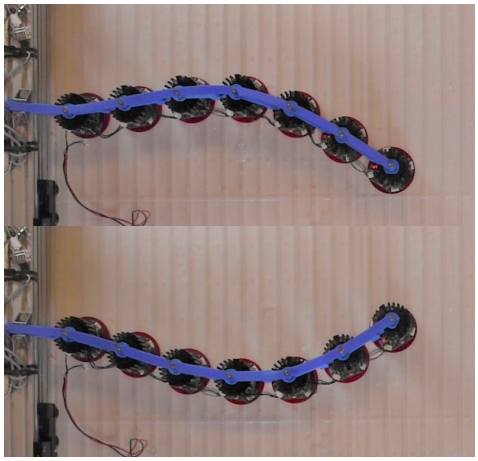

Figure 3-12: The motion stage is programmed to mainly excite the second mode demonstrated by the two extremums.

	Decentralised control	Distributed control
Max τ_n	6.2 mNm	5.0 mNm
$\sum \lvert u_n \rvert$	323 J	395 J
$\sum u_n^2$	53.2	52.5

Table 3-3: Control metrics for the oscillating perturbation given by the motion stage that excited mainly the second mode.

Again it can be concluded that distributed controllers perform better than decentralised as the overall amplification is lower. Besides that, the controllers are more efficient. The maximum control torque in the system is 20% lower than with decentralised controllers. The only downside is that more energy in total is required to achieve this result.

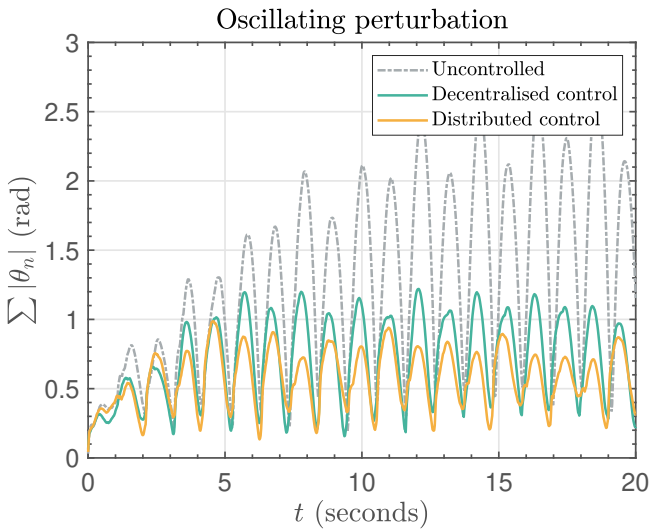

Figure 3-13: Absolute output of all unit cells due to an oscillating perturbation.

Chapter 4

Extending the results

In this section various concepts of LQR and distributed control are further explored. First of all, the results will be extended to a larger robotic cantilever beam. Secondly, the strength of LQR in the Spatial Fourier Domain will be explored, which can be used on periodic robotic meta-structures. For example, many metamaterials are represented as 2D or 3D lattice structures with a hexagonal unit cell. This hexagonal unit cell can be regarded as a periodic system and can be used in conjunction with the Spatial Fourier Domain. Lastly, the Spatial Fourier Domain will be used to tune the closed-loop performance of a large ring of 100 masses.

4-1 Larger pendulum systems

For the robotic cantilever beam with six unit cells, penalisation of the four lower order modes resulted in a clear distributed structure with first neighbour couplings. The question remains whether this conclusion holds for larger systems. The major difference is that larger systems have more actuators and sensors, while the mode shapes remain the same. As a result, more actuator and sensor pairs have the same rotational direction. Consider, for example, the second mode of a robotic cantilever beam of 20 unit cells in Figure 4-1. It contains a large group of over 10 unit cells with the same rotational direction, whereas for the smaller beam this was at most a group of three. The fifth mode for this system still contains many triads with the same rotational direction, while it had strong alternating directions with six unit cells.

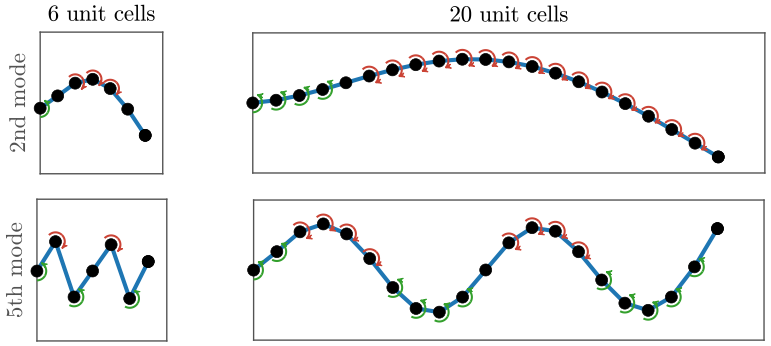

Figure 4-1: 2nd and 5th mode of a robotic cantilever beam with 20 unit cells.

As a result, distributed controllers with first neighbour gains will be beneficial for more modes, because more modes have groups of three unit cells with the same rotational direction. Secondly, for the lowest order modes, for example mode 2, more neighbours are necessary for the optimal control. This is because the size of the groups with the same rotational direction has increased, which also means that more diagonals will be filled with positive gains in the LQR matrix. Consider, for example, three different Q matrices for this robotic beam of 20 unit cells which are all tuned differently for different demands. The first closed-loop is tuned to penalise all modes using $Q = \text{diag}(1, \ldots, 1)$ and $R = 2e6$. The second one focuses mainly on the five lowest order modes, which are heavily penalised with $Q = \text{diag}(1000, 40, 15, 15, 1, \ldots, 1)$ and $R = 3e7$. Lastly, a very specific example that focuses on low-order and mid-order modes with $Q = \text{diag}(500, 40, 20, 20, 15, 15, 15, 15, 15, 15, 1, \ldots, 1)$ and $R = 3e7$.

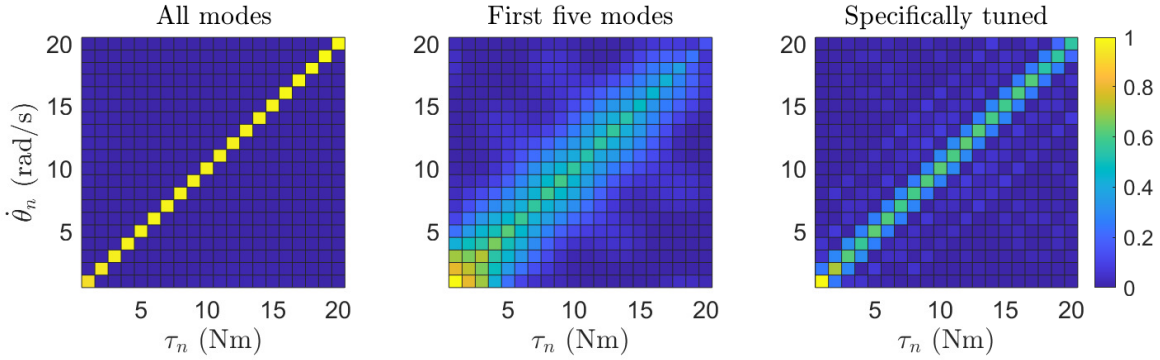

Figure 4-2: Depending on the penalising matrix Q, the amount of neighbours in the results are different.

It can be seen in Figure 4-2 that penalising all modes equally results in a decentralised matrix, which is in accordance to earlier conclusions for the system with six unit cells. By focusing only on the five lowest order modes, the optimal matrix has clear distributed diagonals, but there is a lot more neighbour information required to implement this matrix, namely around three to four neighbours. This seems to be logical when looking at the mode shapes of the system in Figure 4-1. Only through truncation this can be reduced to first neighbour interactions, but this would result in sub-optimal results and perhaps instability. Only if the low-order and mid-order modes are specifically penalised as in example three, a distributed architecture will emerge with only first neighbour couplings. With the currently applied method there is little to no control how many neighbours are included in the feedback matrix. Some form of regularisation or penalisation of entries too far from the diagonal would be necessary if the communication topology doesn't allow for neighbours further away.

The advantage of distributed controllers with more neighbours can be demonstrated with manually derived distributed controllers to avoid truncation and possible stability issues. In Figure 4-3 a decentralised controller, distributed controller with one neighbour and a distributed controller with three neighbours are tested. The frequency response is shown in Figure 4-4. Having at least one neighbour coupling already significantly improves the performance of the system over a decentralised approach for the first seven to eight modes. This demonstrates the feasibility of distributed control for the lower frequency range once again. Furthermore, as expected from the LQR matrices and mode shapes, having more

neighbour couplings results in a slight improvement of the lowest order modes with these larger systems.

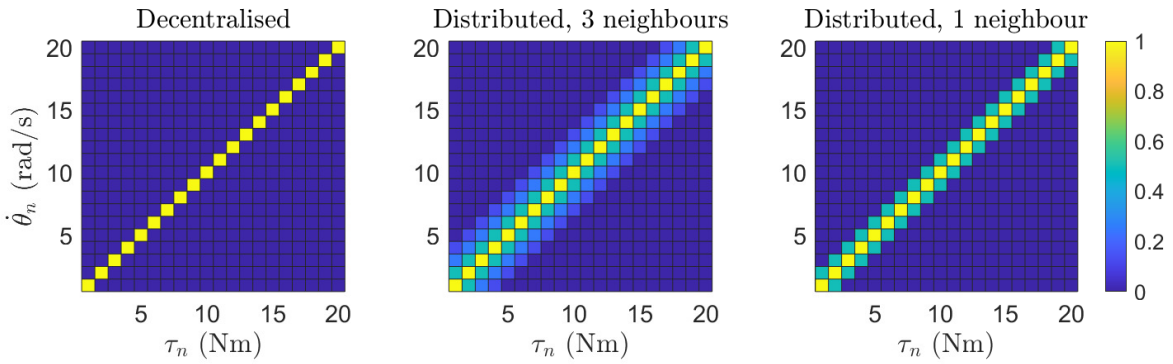

Figure 4-3: Manually tuned decentralised and distributed controllers where all the other gains are set to zero.

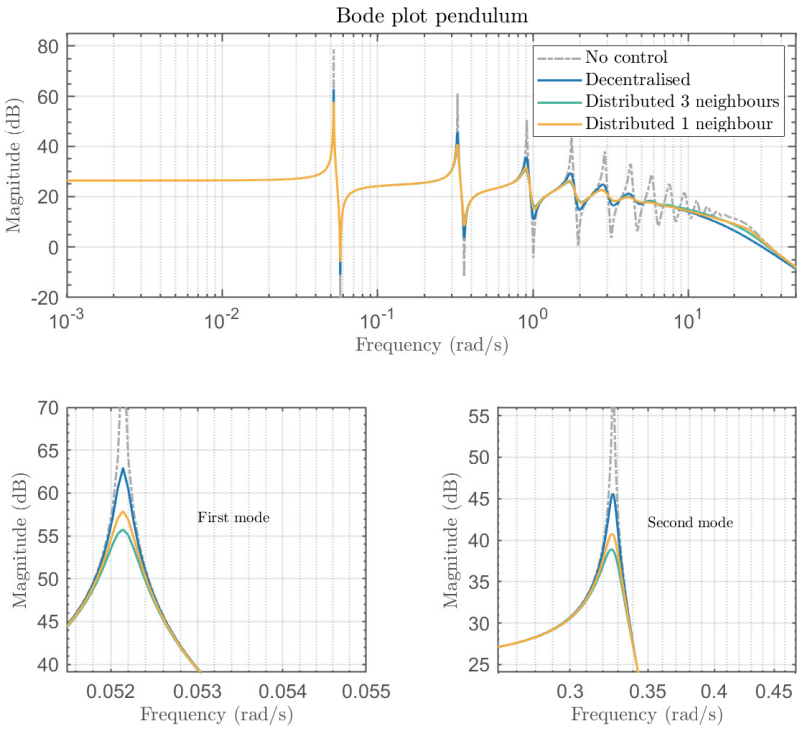

Figure 4-4: Frequency response of the manually tuned systems show that distributed controllers have better damping capabilities than decentralised controllers for the first seven to eight modes of the system.

4-2 Hexagonal structure

The building block for many metamaterial lattice structures is the hexagonal unit cell. Using the torque-actuated joints a hexagonal structure can be constructed where the equilibrium angle between joints is 60 degrees. See Figure 4-5 for a schematic with the relative angles and Figure 4-6 for how the hexagonal would look on the experimental setup.

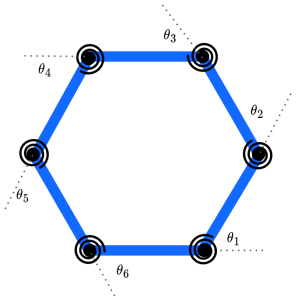

Figure 4-5: Schematic of a hexagonal cell structure that could be used in large lattice structures.

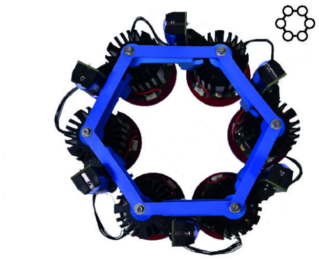

Figure 4-6: Example of the hexagonal structure with the experimental setup [10].

At first, this structure is simplified in modelling by assuming it is a series of six mass-spring systems on a line, where the first and last mass are connected to each other to form a circular arrangement. The equation of motion for any mass in the system can be given by Equation 4-1.

$$m\ddot{x}_n = k(x_{n+1} - x_n) + k(x_{n-1} - x_n) + (u_n - u_{n+1}) + (u_n - u_{n-1}) \tag{4-1}$$

The mass and stiffness matrices are given in Equation 4-2. The first mass is connected to the ground with a very small spring stiffness $\epsilon << k$ to ensure that no rigid body modes are present.

$$M = \begin{bmatrix} \mathrm{m} & 0 & 0 & 0 & 0 & 0 \\ 0 & \mathrm{m} & 0 & 0 & 0 & 0 \\ 0 & 0 & \mathrm{m} & 0 & 0 & 0 \\ 0 & 0 & 0 & \mathrm{m} & 0 & 0 \\ 0 & 0 & 0 & 0 & \mathrm{m} & 0 \\ 0 & 0 & 0 & 0 & 0 & \mathrm{m} \end{bmatrix} \qquad K = \begin{bmatrix} 2\mathrm{k}+\epsilon & -\mathrm{k} & 0 & 0 & 0 & -\mathrm{k} \\ -\mathrm{k} & 2\mathrm{k} & -\mathrm{k} & 0 & 0 & 0 \\ 0 & -\mathrm{k} & 2\mathrm{k} & -\mathrm{k} & 0 & 0 \\ 0 & 0 & -\mathrm{k} & 2\mathrm{k} & -\mathrm{k} & 0 \\ 0 & 0 & 0 & -\mathrm{k} & 2\mathrm{k} & -\mathrm{k} \\ -\mathrm{k} & 0 & 0 & 0 & -\mathrm{k} & 2\mathrm{k} \end{bmatrix} \tag{4-2}$$

As this circular system has spatially invariant dynamics for any number of unit cells, the Spatial Fourier Domain can be used to obtain the optimal feedback matrix with LQR. The Spatial Fourier Transform for a mass-spring system with absolute measurement has already been demonstrated in Section 2 in Equation 2-4. For relative measurements, the transform requires an alteration in the B matrix as shown in Equation 4-3.

$$\begin{bmatrix} \dot{\hat{x}}_\theta \\ \ddot{\hat{x}}_\theta \end{bmatrix} = \begin{bmatrix} 0 & 1 \\ (2\cos(\theta) - 2)k/m & 0 \end{bmatrix} \begin{bmatrix} \hat{x}_\theta \\ \dot{\hat{x}}_\theta \end{bmatrix} + \begin{bmatrix} 0 \\ (2 - 2\cos(\theta))/m \end{bmatrix} \hat{u}_\theta \qquad \text{for} \quad \theta \in [0, 2\pi) \tag{4-3}$$

The ARE is solved algebraically using Matlab to obtain the LQR matrix in Fourier space as function of $Q = \begin{bmatrix} q_1 & 0 \\ 0 & q_2 \end{bmatrix}$, r and the spatial frequency θ, see Equation 4-4.

$$\hat{K} = \left[\sqrt{\frac{q_1}{r} + k^2} - k, \quad \frac{-(2\cos(\theta)-2)\sqrt{(\frac{q_2}{r}(1-\cos(\theta))+m\hat{K}_p}}{2\sqrt{-(\cos(\theta)-1)^3}} \right] \tag{4-4}$$

The inverse of the optimal matrix $\hat{K}$ is obtained by using the inverse formula in Equation 4-5 and using the convolution sum in Equation 4-6 to obtain the full feedback matrix.

$$K = \int_0^{2\pi} \hat{K} e^{j\theta n} \mathrm{d}\theta \tag{4-5}$$

$$u = \sum_{\zeta} K(n-\zeta)x(t,\zeta) \tag{4-6}$$

Conventionally, LQR in the Spatial Fourier Domain penalises the whole frequency range as shown in Section 2, which is unfavourable for AVC applications. In this case, the modes of the system are of interest as well. In this paper we propose two alterations to Equation 4-5 to give more control over the closed-loop frequency response, shown in Equation 4-7.

$$K = \int_{\theta} c(\theta)\hat{K} e^{j\theta n} \mathrm{d}\theta \tag{4-7}$$

The first change concerns the integration bounds for θ, which are made variable. By integrating θ from 0 to 2π the whole frequency range is minimised, which is often unwanted. By integrating closely to 0 and 2π only, the low-frequency range can be targeted. Targeting θ around π, the high-end frequency range is minimised. Due to this alteration, the Spatial Fourier Domain can be used to tune the frequency response of the closed-loop system. For example, for this system it is understood that it exhibits three modes, as it has six unit cells in a circular arrangement. So integrating roughly around $\frac{\pi}{3}$ minimises the first mode, $\frac{2\pi}{3}$ the second and π the third, see Figure 4-7.

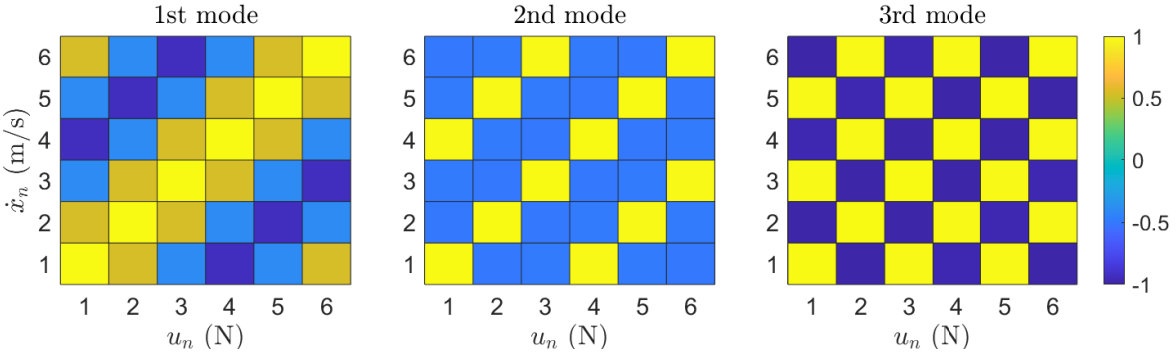

(a) 1st mode obtained by integrating θ from $\frac{\pi}{3} \pm 0.2$.

(b) 2nd mode obtained by integrating θ from $\frac{2\pi}{3} \pm 0.2$.

(c) 3rd mode obtained by integrating θ from $\pi \pm 0.2$.

Figure 4-7: Optimal LQR matrices for each mode, obtained through the Spatial Fourier Domain

It is verified in the modal domain that the LQR matrices are correct. This shows the capability of the Spatial Fourier Domain for circular systems. For any number of unit cells it is possible to obtain closed-loop optimal matrices for different frequency regions.

Besides utilising the Spatial Fourier Domain, the optimal control architecture for this hexagonal system is of interest. Even though the first mode has strong distributed diagonals and a distributed controller seems beneficial, this is deceiving. Since the second and third mode have strong negative gains on the first upper and lower diagonals the optimal control is decentralised. See for example the three feedback matrices in Figure 4-8. The first matrix is fully decentralised, while the second is distributed with positive neighbours and the third is distributed with negative neighbours. In the frequency response in Figure 4-9 the effect of the distributed controllers can be seen. It is clear that positive neighbour gains work well for the first mode, but actually almost destabilise the system due to the third mode amplification. The distributed controller with negative gains works worse for the first and second mode, but better for the last mode. The decentralised controller is the optimal balance between all three modes.

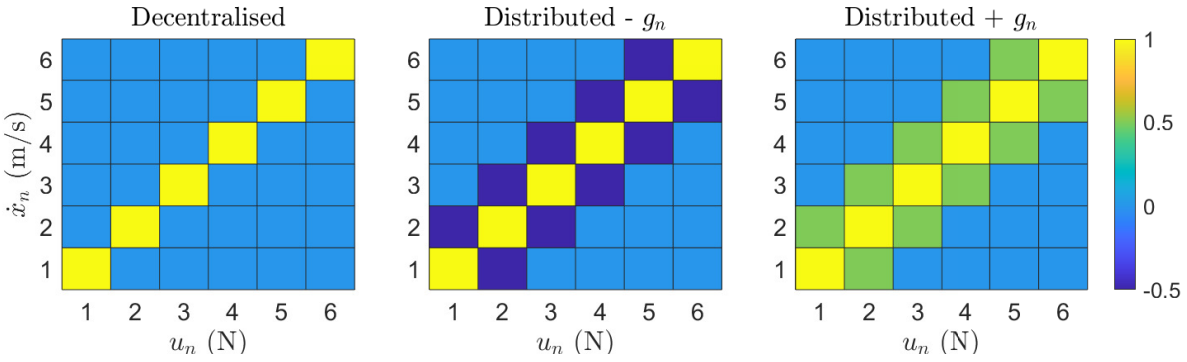

(a) Decentralised controllers.

(b) Distributed controllers with negative neighbour gains.

(c) Distributed controllers with positive neighbour gains.

Figure 4-8: Three different feedback matrices tested on circular mass-spring system.

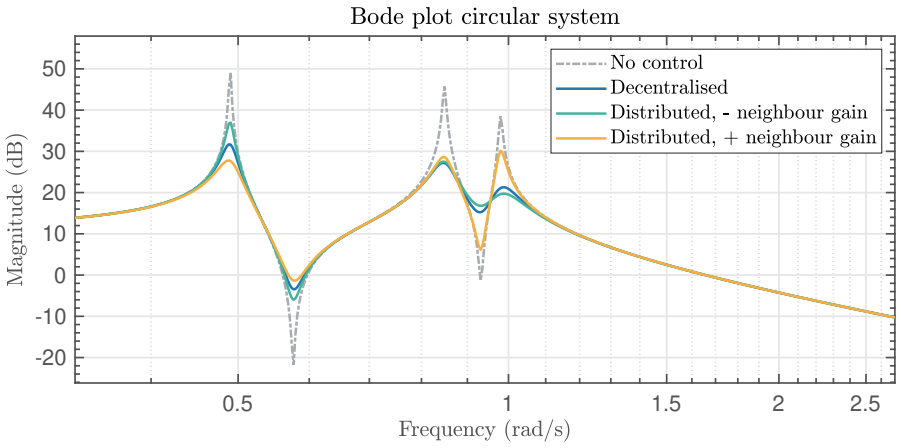

Figure 4-9: Frequency response of the three feedback matrices.

4-3 Larger ring structures

Where the Spatial Fourier Domain reaches its full potential is when the amount of unit cells is increased. This is illustrated for a large ring of 100 unit cells. Doing a modal decomposition for such a large system with 50 modes is excessive and unnecessary. The majority of the work will be done with the Spatial Fourier Transform. It is known from Section 3 that penalising all modes quickly leads to a decentralised matrix. Furthermore, it is also known that lower order modes prefer positive neighbour couplings, whereas higher order modes prefer negative neighbour couplings. All three concepts are confirmed with the following integration bounds:

1. All modes: $0.01 < \theta < 2\pi - 0.01$
2. Higher order modes: $0.8 < \theta < 2\pi - 0.8$
3. Lower order modes: $0.01 < \theta < 0.8 \quad + \quad 2\pi - 0.8 < \theta < 2\pi - 0.01$

The results of the three integration bounds are given in Figure 4-10. It can be seen that penalising all modes indeed results in a fully decentralised matrix. Penalising lower order modes results in a distributed architecture with positive neighbour gains. Distributed control has more of a significance again as more modes are present with distributed diagonals compared to a hexagon. Penalising the high order modes results in a distributed controller as well, but with negative couplings. The strength of the Spatial Fourier Domain is that these optimal solutions can be computed in less than a second, regardless of the size of the system.

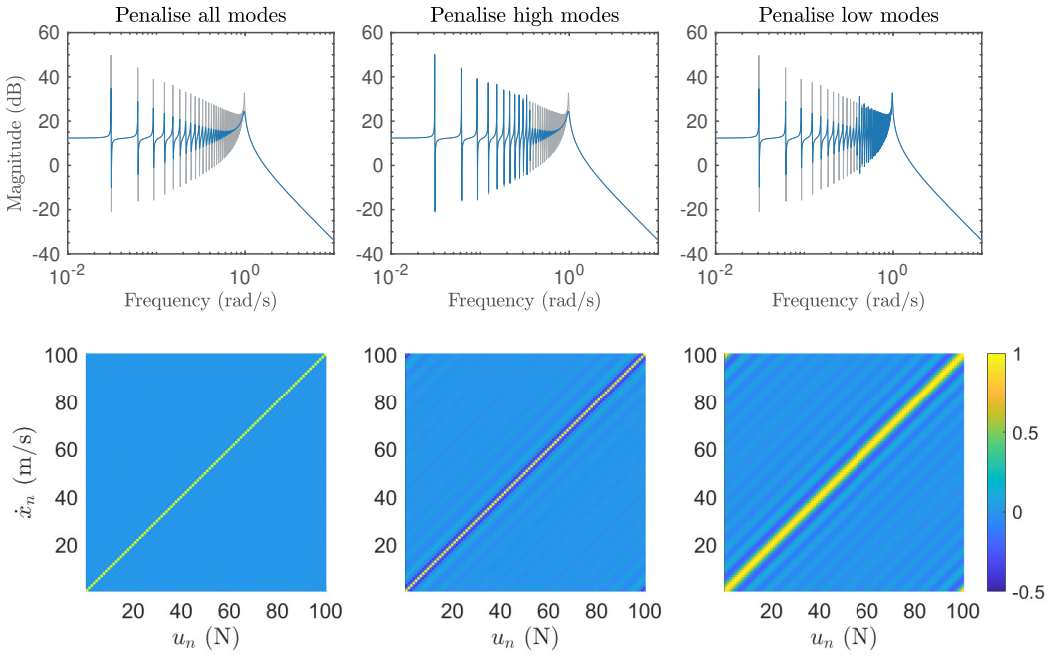

Figure 4-10: Effect of penalising different spatial frequencies for a large ring of 100 masses.

The second alteration we make to the inverse Fourier transform is to include a variable gain $c(\theta)$. Depending on which region of the spatial frequency is integrated, a different gain will be applied. This allows for the same level of flexibility as with the modal domain, while it remains applicable to large systems that are otherwise not solvable. Consider, for example, that lower order modes need to be penalised the most, but higher order modes still require a little bit of damping for stability. This can be done with the gains described in Equation 4-8.

$$\begin{aligned} &\text{if} \quad \theta < 0.6 \quad &\rightarrow \quad K = \int_{\theta} 15\hat{K}e^{j\theta n}\mathrm{d}\theta \\ &\text{if} \quad 0.6 < \theta < 2 \quad &\rightarrow \quad K = \int_{\theta} 10\hat{K}e^{j\theta n}\mathrm{d}\theta \\ &\text{if} \quad 2 < \theta < \pi \quad &\rightarrow \quad K = \int_{\theta} 0.1\hat{K}e^{j\theta n}\mathrm{d}\theta \end{aligned} \tag{4-8}$$

Using this tuning scheme, for any amount of unit cells, the optimal feedback matrix will always be distributed with first neighbour couplings, see Figure 4-11.

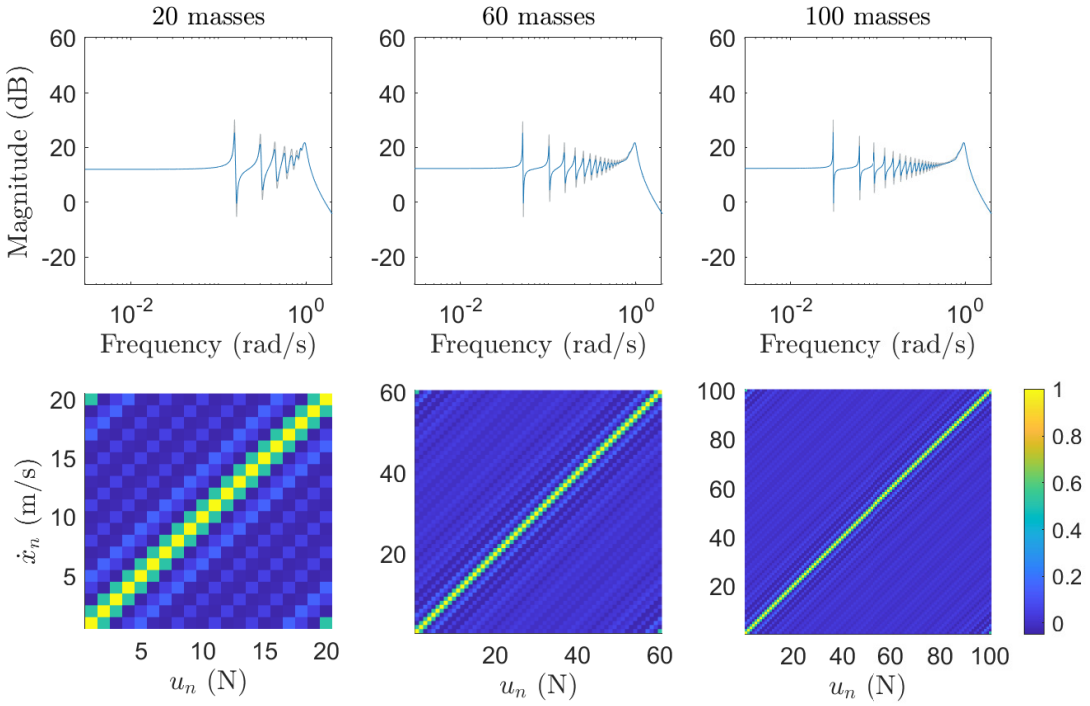

Figure 4-11: With the second alteration to the inverse Fourier Transform, it is possible to tune the closed-loop response of a large periodic system. In this case the tuning parameters result in a distributed matrix with first neighbour couplings.

With this second alteration to the inverse Fourier transform, it is possible to derive intuitive closed-loop characteristics for systems of any size, including infinite systems. And besides that, using the Spatial Fourier Domain, it has been shown that the same conclusions apply for large circular systems. The optimal architecture is decentralised when penalising all modes or distributed with a few neighbour couplings when lower order modes are penalised. Both architectures are practical for implementation into many large-scale structures.

4-4 Matlab model

Although masses on a line are very general and intuitive to derive, the true model of torque-actuated joints is slightly different. Using Simscape Matlab, a model is derived which fully describes the dynamics of masses in a hexagonal arrangement with torque-actuated joints instead of masses on a line with linear forces. From this model it is evident that it behaves exactly the same as the mass-spring system on a line, except that the first mode is not present as it is not controllable. This also holds for larger rings with more unit cells. Hence, for the hexagonal structure, only the last two modes from Figure 4-7 will be present. Combining both modes results in the feedback matrix in Figure 4-12. The result seems promising as it contains clear distributed diagonals. However, as evident from the previous frequency response in Figure 4-9, distributed controllers with negative neighbour gains would only result in a slight improvement in the second mode, while worsening the first mode. Therefore, the conclusion is that decentralised and distributed control architectures perform equally for a torque-actuated hexagon.

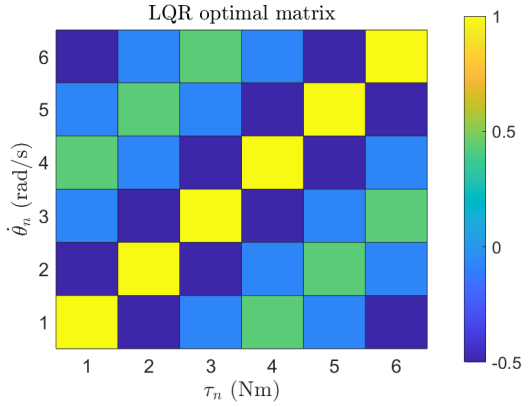

Figure 4-12: LQR optimal matrix obtained through the physical domain with a Simscape model.

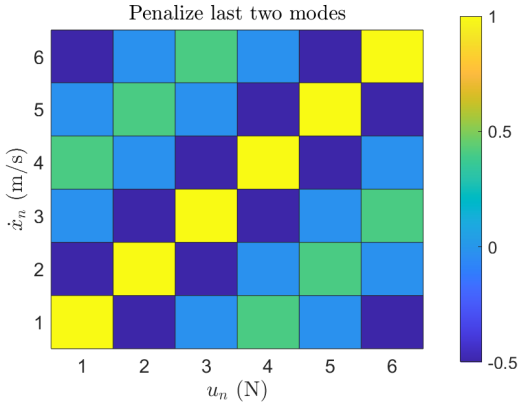

Figure 4-13: LQR optimal matrix obtained through the Spatial Fourier Domain.

To make sure the Spatial Fourier Domain also represents this more accurate model, the only thing that needs to be done is change the integration bounds of θ to exclude the first mode. This is done in Figure 4-13 for the bounds $1.8 < \theta < 2\pi - 1.8$.

Chapter 5

Discussion & Conclusion

In this section, a conclusion is drawn from the results and an answer to the research goal is given. The paper ends with recommendations for future research to improve upon the work done.

5-1 Conclusion

State-of-the-art literature on AVC is predominantly based on centralised and decentralised control architectures. However, for large metamaterials and meta-structures, centralised controllers are impractical to implement and decentralised controllers might lack performance. In literature, distributed control showed optimal performance for spatially invariant systems. This sparked the interest to study distributed control for robotic materials as they are also spatially invariant. However, changes had to be made to incorporate relative measurements and the ability to penalise specific frequency ranges.

In this paper we studied whether a distributed control architecture is advantageous for robotic materials with relative measurements. Furthermore, we looked into different frequency regions to see the effect on the optimal control architecture. The primary system used in this study was a robotic cantilever beam of six unit cells. By penalising the whole frequency range it was shown that the optimal control architecture is decentralised. However, with use of LQR, the modal domain and using the mode shapes of the cantilever beam as a visualisation tool, it was shown that distributed controllers are optimal for damping the first four modes of the system. Compared to decentralised controllers they had superior damping performance, while they remain scalable for implementation in larger systems. This is a significant result as damping of lower order modes is usually more difficult and preferred over higher order modes. Besides that, the maximum actuator force is significantly lower, up to 27% in simulation and 24% in experiments compared to a decentralised solution. This is an important conclusion as many applications are limited by maximum actuator force and miniaturisation of mechatronic devices leads to even smaller and more lightweight actuators.

For a larger cantilever beam of 20 unit cells it was shown that only a specific Q matrix that penalises both low-order and mid-order modes will lead to distributed controllers with first neighbour couplings. For Q matrices with low-order penalisation the optimal control strategy needs multiple neighbours to be close to optimal as the mode shapes are spread over more

actuators and sensors. However, even with a single neighbour, the performance exceeded decentralised control for the low-order and mid-order modes.

From both analyses it can be concluded that distributed control architectures are definitely advantageous for both small-scale and large-scale AVC applications with relative measurements. The strength of the given result in this paper is that it is very universal and can be applied to many different systems. For example, any system that closely resembles a series of mass-spring systems with relative measurements will benefit from this architecture or any other system with similar mode shapes. In addition, the results remain valid for a large range of mass and stiffness values.

Furthermore, the Spatial Fourier Domain was used to study periodic robotic structures. In this paper, an adaption of the inverse Fourier Transform was used, which made it possible to tune the closed-loop performance of periodic rings for different frequency ranges. This gives the Spatial Fourier Domain the same tuning flexibility as the modal domain. Moreover, it allows for tuning of systems that are otherwise not solvable in the modal domain.

For a small hexagonal system it was shown that distributed control wasn't advantageous over decentralised control, as the system only had two modes. For much larger ring structures, however, the same conclusions can be drawn as for the robotic cantilever beam: penalising the whole frequency range results in decentralised architectures, whereas penalising the lower order modes results in distributed architectures.

The results in this paper allow for the further push towards large-scale meta-structures and metamaterials with high performance damping. First of all, the feasibility of a distributed architecture has been proven for systems represented as masses and springs with relative measurements. Also, the value of the Spatial Fourier Domain has been demonstrated as an asset in designing optimal controllers for large-scale robotic metamaterials.

5-2 Further Research

There are a few areas of interest that, with additional research, can elevate the work done in this paper.

The weakness of the modal domain, or LQR in general, is that the optimal structure depends on how you tune the Q matrix. Often the optimal feedback matrices contain too many neighbour couplings or even high off-diagonal entries. Only by carefully tuning the closed-loop system a desired result can be obtained. Otherwise the result has to be truncated, which leads to sub-optimal results and can also lead to unstable systems. A promising alternative solution is to use a regularisation term that forces LQR to find an optimal matrix considering a certain communication topology. For example, if only first neighbour interactions are possible, the regularisation forces the optimal matrix to only find entries for the the diagonal and first upper and lower diagonals. Examples are given in [17] and [12]. Another solution could be to include a masking matrix in the objective function that only allows optimisation of specified entries in the feedback matrix. In addition, it would be valuable to have a metric that specifies how sub-optimal the results are due to the regularisation compared to a full centralised matrix.

For both the robotic cantilever beam and robotic periodic systems, stability is a concern. As the high-frequency modes of these system require strong negative neighbour interactions, a

distributed controller with positive neighbour gains can destabilise the system. Especially when truncating the results of a LQR matrix, this can easily happen. Solutions would be needed to attenuate the higher order modes with filters. Another solution could be to use some form of switching control. This would switch the signs of the neighbour gains from positive to negative based on the frequency range the system is operating in using a frequency estimator.

Besides robotic cantilever beams, further research is needed for 2D lattices. As such systems operate in 2D space, actuators have more than 2 neighbours present for information sharing and the actuators will influence the structure in multiple dimensions as well. Especially for more complex structures, the modal analysis can be used as a good tool to understand if sharing information between neighbours can be beneficial. For example, for a cubic structure where a unit cell has six neighbours, it can be intuitive to understand that only a certain amount of modes will have all six unit cells perturbing in the same direction simultaneously. Many modes will have either one or multiple neighbours moving in opposing directions.

Lastly, further research can be done into translating the given results to continuum structures like cantilever beams with collocated piezoelectric sensors and actuators. It is to be expected that similar conclusions can be reached, since such systems have similar mode shapes with relative measurements. It may not even be needed to implement evenly spaced collocated sensors and actuators. It might already be beneficial to replace large actuators that are placed on locations with maximum modal strain with groups of smaller and cheaper actuators that communicate with each other as it has been demonstrated that distributed control can reach similar or even better performance with lower actuator forces.

Bibliography

[1] K. Verbaan, *Robust Mass Damper Design for Bandwidth Increase of Motion Stages*. 2015.

[2] A. Preumont, "Vibration control of active structures: An introduction," *Meccanica*, vol. 34, pp. 139–139, 1999.

[3] E. Omidi and S. N. Mahmoodi, "Vibration control of collocated smart structures using $\mathcal{H}_\infty$ modified positive position and velocity feedback," *JVC/Journal of Vibration and Control*, vol. 22, pp. 2434–2442, 6 2016.

[4] M. Ahmadian and D. J. Inman, "Adaptive modified positive position feedback for active vibration control of structures," *Journal of Intelligent Material Systems and Structures*, vol. 21, pp. 571–580, 4 2010.

[5] T. van der Graaf, "Active vibration control: Using distributed sensors and actuators," 2021.

[6] M. A. McEvoy and N. Correll, "Materials that couple sensing, actuation, computation, and communication," *Materials science*, vol. 347, 3 2015.

[7] S. Dalela, P. S. Balaji, and D. P. Jena, "A review on application of mechanical metamaterials for vibration control," *Mechanics of Advanced Materials and Structures*, pp. 1–26, 2 2021.

[8] Y. Song, P. C. Dohm, B. Haghpanah, A. Vaziri, and J. B. Hopkins, "An active microarchitectured material that utilizes piezo actuators to achieve programmable properties," *Advanced Engineering Materials*, vol. 18, pp. 1113–1117, 7 2016.

[9] Y. Song, "Design and optimization of active microarchitectured metamaterials," 2018.

[10] M. Brandenbourger, C. Scheibner, J. Veenstra, V. Vitelli, and C. Coulais, "Active impact and locomotion in robotic matter with nonlinear work cycles," 8 2021.

[11] M. Brandenbourger, X. Locsin, E. Lerner, and C. Coulais, "Non-reciprocal robotic metamaterials," *Nature Communications*, vol. 10, 12 2019.

[12] M. R. Jovanović and N. K. Dhingra, "Controller architectures: Tradeoffs between performance and structure," vol. 30, pp. 76–91, European Control Association, 7 2016.

[13] B. Bamieh, F. Paganini, and M. A. Dahleh, "Distributed control of spatially invariant systems," *IEEE Transactions on Automatic Control*, vol. 47, pp. 1091–1107, 7 2002.

[14] R. D'Andrea and G. E. Dullerud, "Distributed control design for spatially interconnected systems," *IEEE Transactions on Automatic Control*, vol. 48, pp. 1478–1495, 9 2003.

[15] M. R. Jovanović and B. Bamieh, "On the ill-posedness of certain vehicular platoon control problems," *IEEE Transactions on Automatic Control*, vol. 50, pp. 1307–1321, 9 2005.

[16] M. R. Jovanović and B. Bamieh, "Lyapunov-based output-feedback distributed control of systems on lattices," vol. 2, pp. 1333–1338, 2003.

[17] M. R. Jovanoví, "On the optimality of localised distributed controllers," 2010.

[18] A.-K. Schug, S. Heinke, and H. Werner, *Distributed Control of Large Scale Interconnected Systems with Boundary Conditions-Shift Operator vs. Interconnection Graph.* 2020.

[19] S. M. Ginta, A. K. Schug, and H. Werner, "A decomposition approach for a class of spatially interconnected systems of finite spatial extent," vol. 2018-June, pp. 949–954, Institute of Electrical and Electronics Engineers Inc., 8 2018.

[20] C. Langbort and R. D'Andrea, "Distributed control of spatially reversible interconnected systems with boundary conditions," *SIAM Journal on Control and Optimization*, vol. 44, pp. 1–28, 2006.

[21] M. R. Jovanović and B. Bamieh, "Lyapunov-based distributed control of systems on lattices," *IEEE Transactions on Automatic Control*, vol. 50, pp. 422–433, 4 2005.

[22] J. N. Callen, "Distributed control for unmanned vehicles."

[23] M. I. Hussein and M. J. Frazier, "Metadamping: An emergent phenomenon in dissipative metamaterials," *Journal of Sound and Vibration*, vol. 332, pp. 4767–4774, 9 2013.

Appendix A

System model

The displacements can algebraically be setup for any N with the following equation. Note that u_N is the added mass that is not controlled. The first unit cell u_0 has displacement zero and is not included in the displacements.

$$\boldsymbol{u} = \begin{bmatrix} u_{1,x} \\ u_{1,y} \\ u_{2,x} \\ u_{2,y} \\ \vdots \\ u_{N-1,x} \\ u_{N-1,y} \\ u_{N,x} \\ u_{N,y} \end{bmatrix} = l \begin{bmatrix} 1 & 0 & 0 & 0 & \dots & 0 & 0 & 0 & 0 \\ 0 & 1 & 0 & 0 & \dots & 0 & 0 & 0 & 0 \\ 1 & 0 & 1 & 0 & \dots & 0 & 0 & 0 & 0 \\ 0 & 1 & 0 & 1 & \dots & 0 & 0 & 0 & 0 \\ \vdots & \vdots & \vdots & \vdots & \ddots & \vdots & \vdots & \vdots & \vdots \\ 1 & 0 & 1 & 0 & \dots & 1 & 0 & 0 & 0 \\ 0 & 1 & 0 & 1 & \dots & 0 & 1 & 0 & 0 \\ 1 & 0 & 1 & 0 & \dots & 1 & 0 & 1 & 0 \\ 0 & 1 & 0 & 1 & \dots & 0 & 1 & 0 & 1 \end{bmatrix} \begin{bmatrix} \cos\left(\sum_1^1 \theta_n\right) \\ \sin\left(\sum_1^1 \theta_n\right) \\ \cos\left(\sum_1^2 \theta_n\right) \\ \sin\left(\sum_1^2 \theta_n\right) \\ \vdots \\ \cos\left(\sum_1^{N-1} \theta_n\right) \\ \sin\left(\sum_1^{N-1} \theta_n\right) \\ \cos\left(\sum_1^N \theta_n\right) \\ \sin\left(\sum_1^N \theta_n\right) \end{bmatrix} \tag{A-1}$$

Through the given equations in Section 3-1, the following M and K matrices are obtained for a system with 6 unit cells:

$$M = ml^2 \begin{bmatrix} 91 & 70 & 50 & 32 & 17 & 6 \\ 70 & 55 & 40 & 26 & 14 & 5 \\ 50 & 40 & 30 & 20 & 11 & 4 \\ 32 & 26 & 20 & 14 & 8 & 3 \\ 17 & 14 & 11 & 8 & 5 & 2 \\ 6 & 5 & 4 & 3 & 2 & 1 \end{bmatrix} \qquad K = \begin{bmatrix} k & 0 & 0 & 0 & 0 & 0 \\ 0 & k & 0 & 0 & 0 & 0 \\ 0 & 0 & k & 0 & 0 & 0 \\ 0 & 0 & 0 & k & 0 & 0 \\ 0 & 0 & 0 & 0 & k & 0 \\ 0 & 0 & 0 & 0 & 0 & k \end{bmatrix} \tag{A-2}$$

The damping is added similarly as the stiffness matrix, where the value of $4 \cdot 10^{-4}$ is chosen to have presence of all 6 modes and for stability in the numerical simulation.

$$C = 4 \cdot 10^{-4} \begin{bmatrix} 1 & 0 & 0 & 0 & 0 & 0 \\ 0 & 1 & 0 & 0 & 0 & 0 \\ 0 & 0 & 1 & 0 & 0 & 0 \\ 0 & 0 & 0 & 1 & 0 & 0 \\ 0 & 0 & 0 & 0 & 1 & 0 \\ 0 & 0 & 0 & 0 & 0 & 1 \end{bmatrix} \tag{A-3}$$

The state space of the system can be filled in with the M, C and K matrices as follows:

$$\dot{x} = \begin{bmatrix} \mathbf{0} & \mathbf{I} \\ -\mathbf{M}^{-1}\mathbf{K} & -\mathbf{M}^{-1}\mathbf{C} \end{bmatrix} x + \begin{bmatrix} \mathbf{0} \\ \mathbf{M}^{-1} \end{bmatrix} u \tag{A-4}$$

$$y = \begin{bmatrix} \mathbf{I} & \mathbf{0} \\ \mathbf{0} & \mathbf{I} \end{bmatrix} x \tag{A-5}$$

Appendix B

Additional plots

Truncation

It can be seen that the truncation of the optimal LQR matrix hasn't lead to a significant performance decrease. The decentralized controller still performs worst as the magnitude of vibrations are high and decay the slowest. The distributed velocity feedback controllers perform better than decentralized ones and mostly equal to the fully centralized matrix.

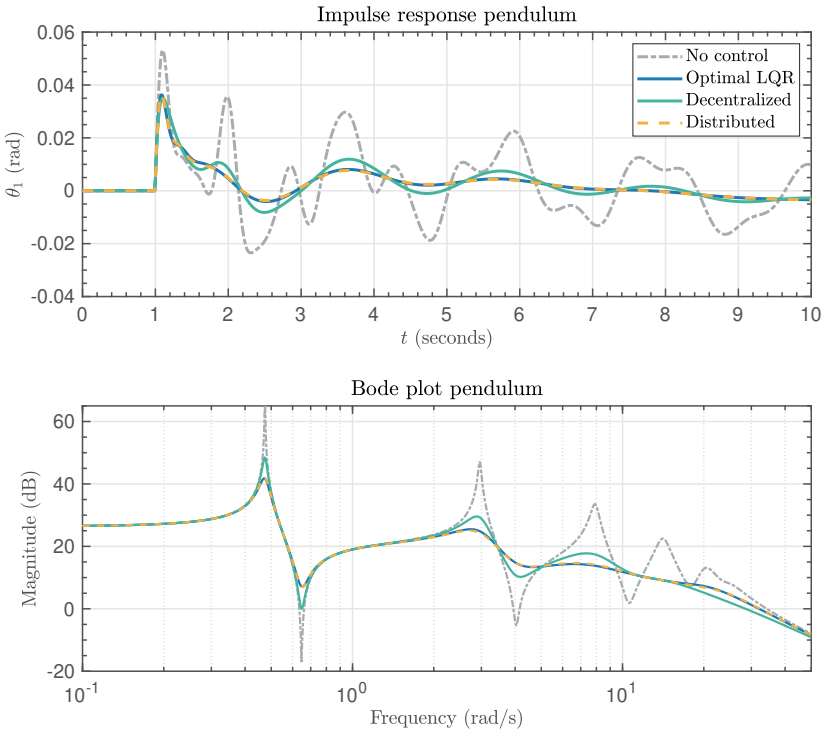

Figure B-1: Performance of truncated optimal controllers.

Stability

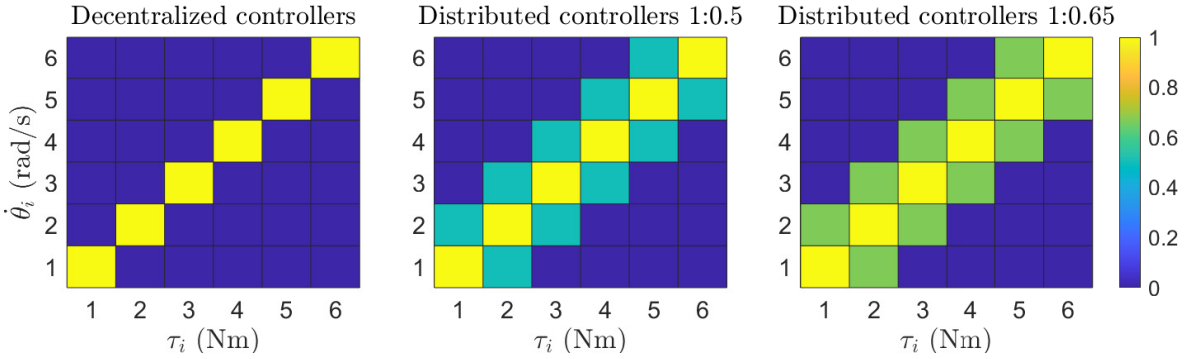

(a) Optimal centralized LQR matrix.

(b) Modular decentralized controllers.

(c) Modular distributed controllers.

Figure B-2: Feedback matrices where every controller has the same gain are compared to an optimal centralized matrix.

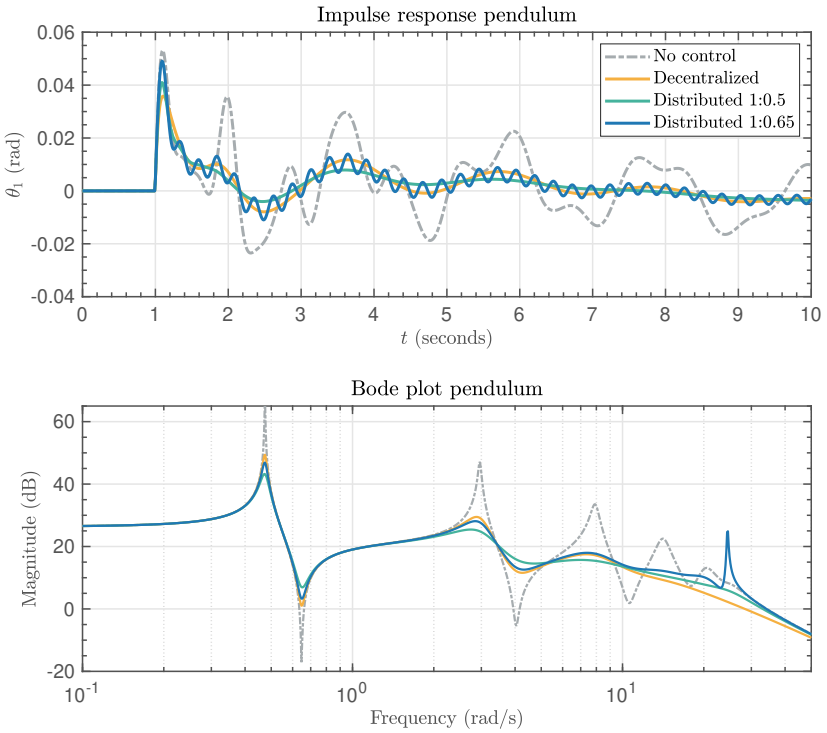

Figure B-3: Time response of three closed-loop systems. Choosing the neighbour gain too high can destabilise the higher order modes.

Experiments

The experiments for the step response were repeated three times to ensure the variance between different experiments was low. As can be seen from both figures, the trials were almost identical, ensuring that the variance between comparisons is low.

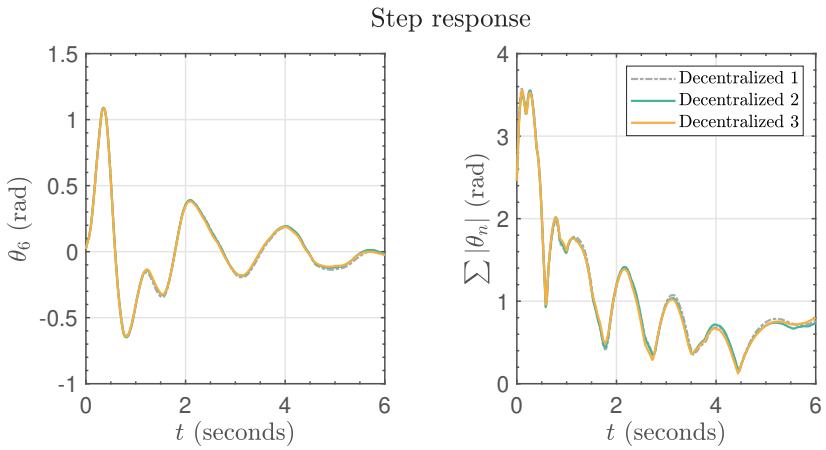

Figure B-4: Variance between the decentralized controllers

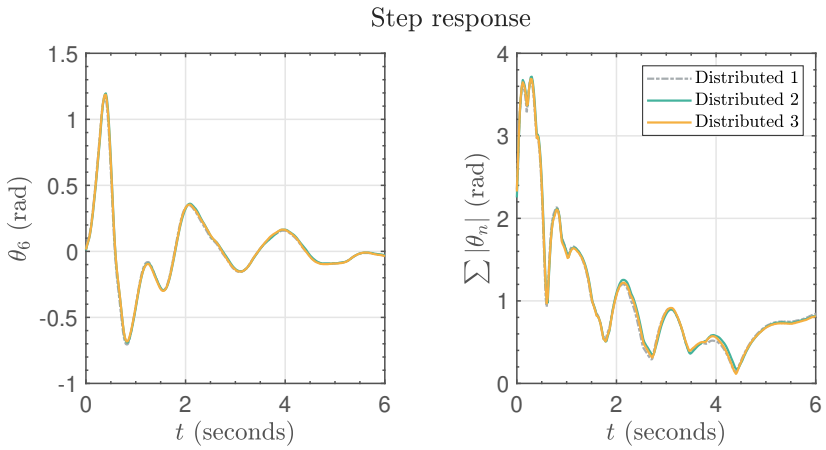

Figure B-5: Variance between the distributed controllers

Appendix C

Actual gains used

The feedback matrices are normalized to make sure the colour gradient is comparable between different feedback matrices. However, for feedback matrices that are compared to each other in impulse responses or frequency responses, the actual maximum gains are important for reference and are given in the following table:

Figure		Max value
Figure 2-3	left	0.3
Figure 2-3	right	0.00072
Figure 2-4	left	0.297
Figure 2-4	right	0.0038
Figure 3-2	left	0.316
Figure 3-2	right	0.0096
Figure 3-4	left	0.0042
Figure 3-4	right	0.0082
Figure 4-3	left	0.002
Figure 4-3	middle	0.0021
Figure 4-3	right	0.0021
Figure 4-8	left	0.0158
Figure 4-8	middle	0.0118
Figure 4-8	right	0.0200